We are IntechOpen, the world's leading publisher of Open Access books Built by scientists, for scientists

6,900
Open access books available

185,000
International authors and editors

200M
Downloads

Our authors are among the

154
Countries delivered to

TOP 1%
most cited scientists

12.2%
Contributors from top 500 universities

CLARIVATE ANALYTICS
BOOK CITATION INDEX
INDEXED

WEB OF SCIENCE™

Selection of our books indexed in the Book Citation Index
in Web of Science™ Core Collection (BKCI)

Interested in publishing with us?
Contact book.department@intechopen.com

Numbers displayed above are based on latest data collected.
For more information visit www.intechopen.com

4

Semiconducting Oxide Nanowires: Growth, Doping and Device applications

Qing Wan[1,2], Jia Sun[2] and Huixuan Liu[2]
[1]Ningbo Institute of Materials Technology and Engineering,
Chinese Academy of Sciences, Ningbo,
[2]Key Laboratory for Micro-Nano Optoelectronic Devices of Ministry of Education,
Hunan University, Changsha,
[1,2]People's Republic of China

1. Introduction

During the past decade, semiconducting oxide nanowires have been extensively investigated due to their unique features, such as the ultrahigh surface-to-volume ratios, quantum confinement effect, less scattering of the carrier, and higher mobilities compared to their bulk counterparts. These extraordinary properties of semiconducting oxide nanowires have led many researchers to pursue synthesis, doping, and novel device applications, due to their potential applications in nanoscale electronic and optoelectronic devices [1-23]. Such applications include high-performance nanowire-based field-effect transistors (FETs) [1-11], sensors [12-21] and vacuum electron field emitters [22-29], etc.

This chapter provides a comprehensive perspective on research efforts made on synthesis, doping, and device applications of semiconducting oxide nanowires. The contents have been divided into three sections. The first part briefly introduces the synthesis of semiconducting oxide nanowires. The second part introduces the doping schemes of semiconducting oxide nanowires, and then studied the electrical and optical properties of the doped nanowires. The last part mainly describes the applications of semiconducting oxide nanowires, such as FETs, sensors and field emission.

2. Semiconducting oxide nanowires growth

Up to now, many techniques have been developed in the synthesis of semiconducting oxide nanowires. Basically, they can be described as two different types: the ''top-down'' approaches and the ''bottom-up'' approaches. The growth techniques of nanowires discussed in this section are based primarily on bottom- up approaches. As compared with top-down techniques, the bottom-up approaches would go far beyond the limits of top-down technology in terms of future physical and economic limits [30]. Therefore, they are capable of creating nanoscale features. In general, a self-assembly growth could be a self-limited process. For example, it could be a growth spatially defined by the template or a self-ordering process established on a dynamic balance of two opposite physical or chemical interactions such as attractive and repulsive forces, diffusion and dissolution, and so on.

2.1 Growth mechanisms

The growth mechanisms for the most of semiconducting oxide nanowires include vapor-liquid-solid (VLS), vapor-solid (VS) mechanisms and so on.

2.1.1 VLS mechanism

Among the various mechanisms for the growth of semiconducting oxide nanowires, VLS mechanism is the well established and the most widely accepted model. As mentioned, the VLS mechanism was reported by Wagner and Ellis in the mid-1960s to explain the growth of Si whiskers using Au as a metal catalyst [31]. The name of VLS mechanism refers to the fact that the source material from the vapor passes through a liquid droplet and finally ends up as a solid. So, the VLS process can be divided into three steps. The first step is the formation of the liquid alloy droplet which contains Au catalyst and source materials. The second step is the crystal nucleation upon gas adsorption and supersaturation. The last step is the axial growth from the crystalline seeds to form nanowires [32]. Figure.1 illustrates the growth of nanowires by a VLS process [6]. According to the VLS mechanism, we know that the liquid phase is formed initially due to the presence of a low-melting-point phase in an alloy system which consists of the substrate and gas phase constituent. The liquid surface adsorbs the reactant gaseous species much more efficiently than does the solid surface. On supersaturation of the liquid alloy, a nucleation center forms and serves as a preferred site for the axial growth of the nanowires. The adsorbed gas reactants then diffuse through the liquid phase to the solid-liquid interface, resulting in the growth of the solid phase. The growth at the solid-liquid interface is much faster than at the solid-vapor interface due to the much larger accommodation coefficient of the reactants in the liquid [33-34]. During this process, a vapor phase reactant is solubilized by a liquid catalyst particle to form solid wire-like structures and the catalyst is envisioned as growths site that defines the diameter of nanowires. Therefore, the characteristic of VLS growth is the existence of gold nanoparticles on the top of the obtained nanowires [35], typically observed by transmission electron microscopy as shown in Fig.2. At the same time, the diameter of the nanowires is well controlled by the size of the gold nanoparticle as a result of the fact that the diameter of a nanowire via VLS growth is primarily determined by the liquid alloy droplet.
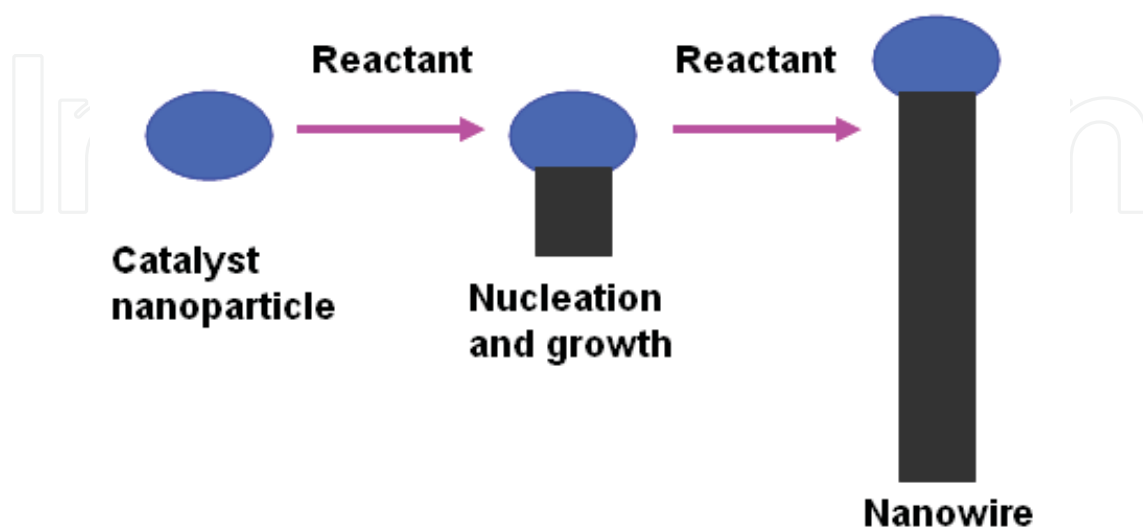

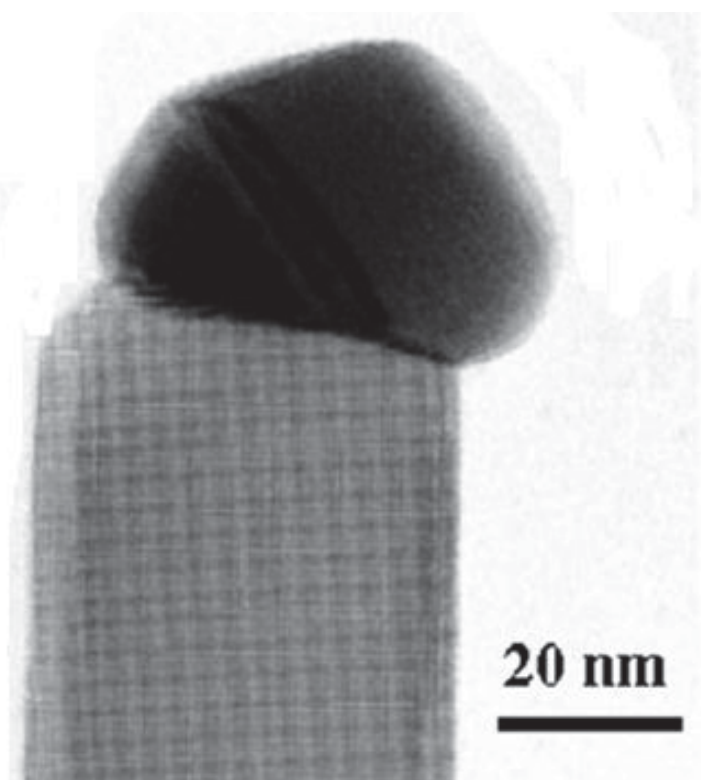Fig. 1. Schematic illustrations of the growth process for a VLS process.

Fig. 2. TEM image of a tin-doped indium oxide nanowire grown along the (001) direction. (From ref. [35])

2.1.2 VS mechanism
VS mechanism is a catalyst-free process that forms nanowires. It involves the direct vaporization of the solid at a higher temperature followed by the deposition of the nanowires at a lower temperature. During VS growth, no catalyst is used and the nanowires are directly grown on the solid particles. This simple method has been widely used to synthesize a lost of semiconducting oxide nanowires [12, 36-37].

2.2 Growth techniques
Semiconducting oxide nanowires with various compositions have been synthesized using a wide variety of methods, from the simple thermal evaporation to the complicated epitaxial growth techniques. Table 1 gives a summary of the methods and mechanisms for semiconducting oxide nanowires growth. The common technique reported is vapor phase transport, including thermal evaporation, pulse laser deposition and chemical vapor deposition (CVD) [38-39]. Other techniques include template-assisted growth [40] and solution synthesis [41]. We devote our most attention to vapor phase transport and thermal evaporation methods.

Materials (nanowire)	Growth method	Growth mechanism	Ref
ZnO	Directly evaporation	VS	36,37,12,43, 45,46
Cd-ZnO	Thermal evaporation	VS	42,44
SnO_2	Laser ablation	VLS	49
SnO_2	Thermal evaporation	VLS	47
Sb-SnO_2	Thermal evaporation	VLS	48,52,54,55,18
Sb-SnO_2	Vapor-transport	VLS	10, 11, 56
Ta-SnO_2	Vapor-transport	VLS	53
In_2O_3	Laser ablation	VLS	50
Sn-In_2O_3	Vapor-transport	VLS	35
Sn/Mo-In_2O_3	Vapor-transport	VLS	51
Vertically aligned Sn-In_2O_3	Thermal evaporation	VLS	23
β-Ga_2O_3	Chemical vapor deposition	VLS	38
$ZnGa_2O_4$	Chemical vapor deposition	VLS	39

Table 1. A summary of the methods and mechanisms for semiconducting oxide nanowires growth

2.2.1 Vapor Phase Transport

Vapor phase transport (VPT) is an atomic deposition process. During this process, source species physically or chemically vaporized from a solid source are transported onto a substrate where they condenses and deposits. According to the approaches for the source vaporization, vapor phase transport can be in the form of thermal evaporation [42-48] and laser ablation [49-50]. When the source species are gas, evaporating liquids or chemically gasified solids, the deposition process is categorized as chemical vapor deposition [38-39]. So far, a majority of the vapor deposition techniques have been developed for the growth of single-crystal semiconducting oxide nanowires. The growth mechanism of VPT has been attributed to either VLS or VS, depending on whether the metal catalysts are presented or not.

2.2.2 Thermal evaporation

Thermal evaporation is one of the simplest methods available to synthesize semiconducting oxide nanowires. Deposition of nanowires occurs on the substrates placed downstream of the carrier gas (such as nitrogen and argon).

2.3 Summary

Among various growth mechanisms, the VLS mechanism has been combined with a wide variety of growth techniques, including catalyst-assisted thermal evaporation, solution and VPT method. Through carefully controlled growth conditions, the vertically aligned tin-doped indium oxide nanowire arrays have been demonstrated using the thermal evaporation. The solution growth method is of low cost, however it is complicated in terms of the control of the growth process. So far, VPT is the widely adopted method, probably due to the simplicity of the required facilities. At the same time, the VLS growth also leads to the incorporation of doping impurities in the as-grown semiconducting oxide nanowires.

3. Doping of semiconducting oxide nanowires

3.1 Doping

Doping in semiconductor has been a very well established process. The doping means the introduction of impurity atoms in a semiconductor, which is fundamental to the control of the bulk properties of a semiconductor. Impurity atoms incorporated into a semiconductor can only exist in two ways. For the first case, the impurity atoms replace the semiconductor atoms at their lattice positions. While for the second case, the impurity atoms exit the semiconductor atoms at their lattice of gap positions, which is a gap type of doping. Generally, the size of the replace atoms is similar to the size of substituted semiconductor atoms, while the size of gap atoms is much smaller. Figure.3 shows the schematics for a replace impurity atom and a gap impurity atom.
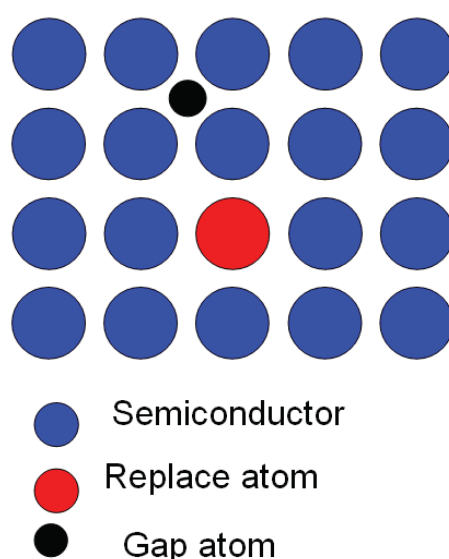
Fig. 3. The schematics for a replace impurity atoms and gap impurity atoms.

With the incorporation of donors, a semiconductor becomes an n-type conductor. While with the incorporation of acceptors, the semiconductor becomes a p-type conductor. Whether the dopants successfully change the density of carriers or not depends on not only the energy of the electrons in the dopant atom but also the temperature. Incorporation of both donors and acceptors in a semiconductor does not lead to the increased concentrations of both electrons and holes since the density of the electrons and the density of holes are equal to the intrinsic density in the doped semiconductors. Typical doping concentrations are in the range of $10^{15}/cm^3$ to $10^{19}/cm^3$. This is relatively small as compared with the density of lattice atoms, which is about $10^{23}/cm^3$. The introduction of intentional impurities or dopants to control the behaviors of materials lies at the heart of many technologies. The impurity doping is an effective method for manipulating the physical properties of semiconductors, including the electronic, optical, and magnetic properties. A substitutional impurity with one more valence electron than the host atom it replaces can be ionized by thermal energy and donate its extra electron to the semiconductor (n-type doping). Similarly, an impurity with one less valence electron can provide an extra hole (p-type doping). These electrons and holes are then available as carriers of a electrical current. Since a thin conducting film is required for the applications of the nanocrystals, the ability to introduce these carriers is becoming important. So, doping process is critical for semiconductors. For these reasons, researchers have begun to

explore the effects of dopants on the semiconductor nanocrystals with unusual and size-specific electronic, optical, and magnetic behaviors. However, extending doping process from films to nanoscale counterparts still remains a big challenge because of both fundamental synthetic issues and "self-purification" mechanisms. Moreover, dopants in nanocrystals are also expected to exhibit phenomena not found in the bulks since their electronic states are confined to a small volume.

3.2 The electrical properties of the doped semiconducting oxide nanowires
3.2.1 Tin-doped indium oxide

For unintentionally doped semiconducting oxide nanowires, the carriers are normally generated by structural defects such as oxygen deficiencies. As a result, the devices behave as wide band gap semiconductors whose performance is influenced by the surrounding environment. On the other hand, intentional doping can greatly modify the device properties and yield new device applications. One such example is tin-doped indium oxide (ITO), in which metal-like behavior is achieved when In_2O_3 is degenerately doped by Sn. Due to its high conductivity and high transmittance in the visible spectral region, ITO has become by far the most important transparent conducting oxide material, and ITO films have found applications in various optoelectronic devices such as flatpanel displays, solar cells, and light-emitting diodes. The ability to obtain highly transparent and highly conducting ITO nanowires may potentially further enhance the performance of such devices due to the increased effective device area using nanowire electrodes. Furthermore, the highly conducting ITO nanowires may also be used as interconnects in integrated nanocsale devices.

The growth of ITO nanowires/nanorods has been reported by several groups since the first study on semiconducting oxide nanobelts in 2001.[57] However, detailed electrical characterization was rarely reported, and it is not clear whether these ITO nanowire/nanorods have the desired electrical properties. In 2004, Q. Wan et.al. reported the resistivity value of ITO nanowires to be ~0.4 $\Omega\cdot$cm [58]. Subsequently, they optimized the doping growth and electrical characterization, the lowest resistivity value of the individual ITO nanowire was estimated to be 6.29×10^{-5} $\Omega\cdot$cm, which is comparable to the best values achieved in high-quality ITO films.[23, 35,51]

The electrical transport properties of the ITO nanowires were studied on devices consisting of individual nanowires. The nanowires were first removed from the growth substrate by sonication in isopropyl alcohol and deposited onto a degenerately doped n-type silicon substrate capped with a 50 nm silicon dioxide layer. Photolithography or electron-beam (e-beam) lithography processes were used to define pairs of metal electrodes on the SiO_2/Si substrate, followed by metal deposition of Ti/Au (10 nm/100 nm) by electron beam evaporation to complete the device structure. Prior to metal evaporation, the samples were cleaned with O_2 plasma (50 W, 30−60 s) to remove possible resist residue. Postannealing processes were not performed in the devices.

More than 40 ITO nanowire devices were fabricated and the electrical properties of individual nanowires were investigated both in ambient air and in vacuum (5×10^{-5} Torr). A linear current (Ids) versus voltage (Vds) curve (Figure 4a) was observed in all measurements and on samples defined by photolithography as well as e-beam lithography methods. This indicates that good Ohmic contacts can be readily achieved between the ITO nanowire and Ti/Au electrodes. To further characterize this observation, four-probe measurements were carried out to study the effects of the contacts. As shown in Figure 4a, the I_{ds}−V_{ds} curve obtained from the four-probe method is almost identical to that obtained from the two-probe method using the inner pair of electrodes.
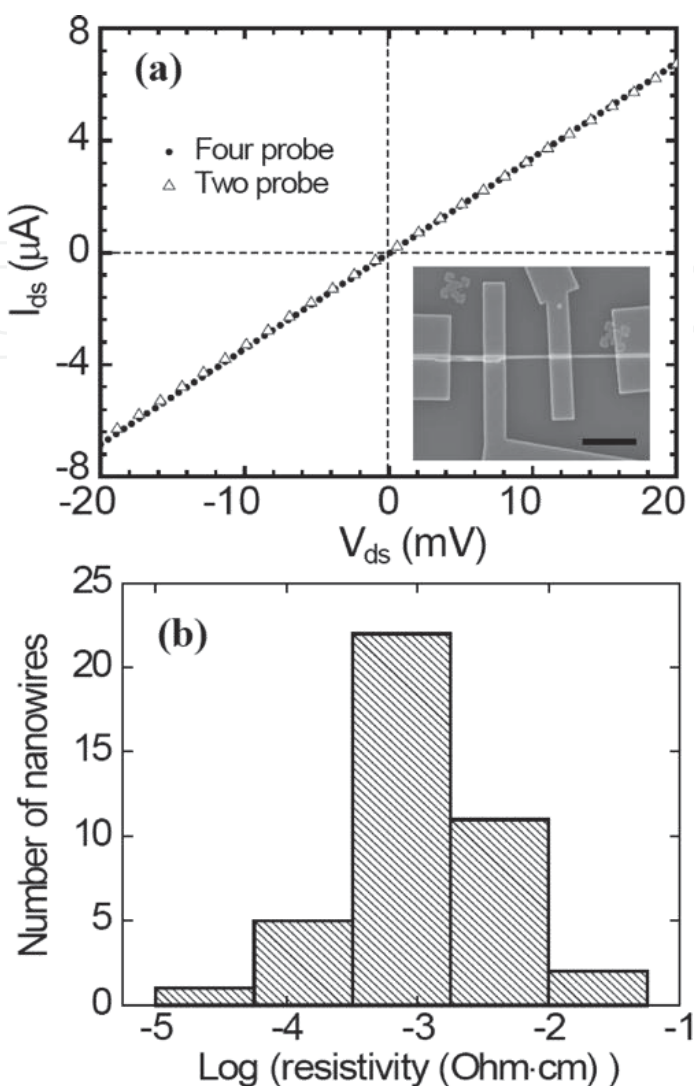
Fig. 4. (a) Comparison of the current−voltage characteristics of an individual ITO nanowire using four-probe and two-probe configurations. Inset, SEM image of the ITO nanowire device. Scale bar: 2 µm. (b) Histogram of the resistivities measured over 40 ITO nanowire.

The small difference between the measured resistances 2936 Ω (four-probe) and 2984 Ω (two-probe) can be mostly attributed to the resistance of the metal leads (≈55 Ω) connecting the nanowire devices to the contact pads, and verifies that contacts to the ITO nanowires are indeed Ohmic with negligible values of resistance. The ability to produce reliable Ohmic contacts is very desirable in nanoscale device applications and also affords us to focus our studies on the simpler two-probe device structure in the following discussions. From the measured resistance value of the device in Figure 4a and the cross-section size (75 nm) and the length (1.8 µm) of the ITO nanowire (measured by SEM imaging), we can calculate the resistivity of the ITO nanowire to be 9.18×10^{-4} Ω·cm. The resistivities of about 40 ITO nanowires were obtained and plotted in Figure 4b. Significantly, the median resistivity value 7.15×10^{-4} Ω·cm, and lowest resistivity value 6.29×10^{-5} Ω·cm, are comparable to the best values achieved in high-quality ITO films.
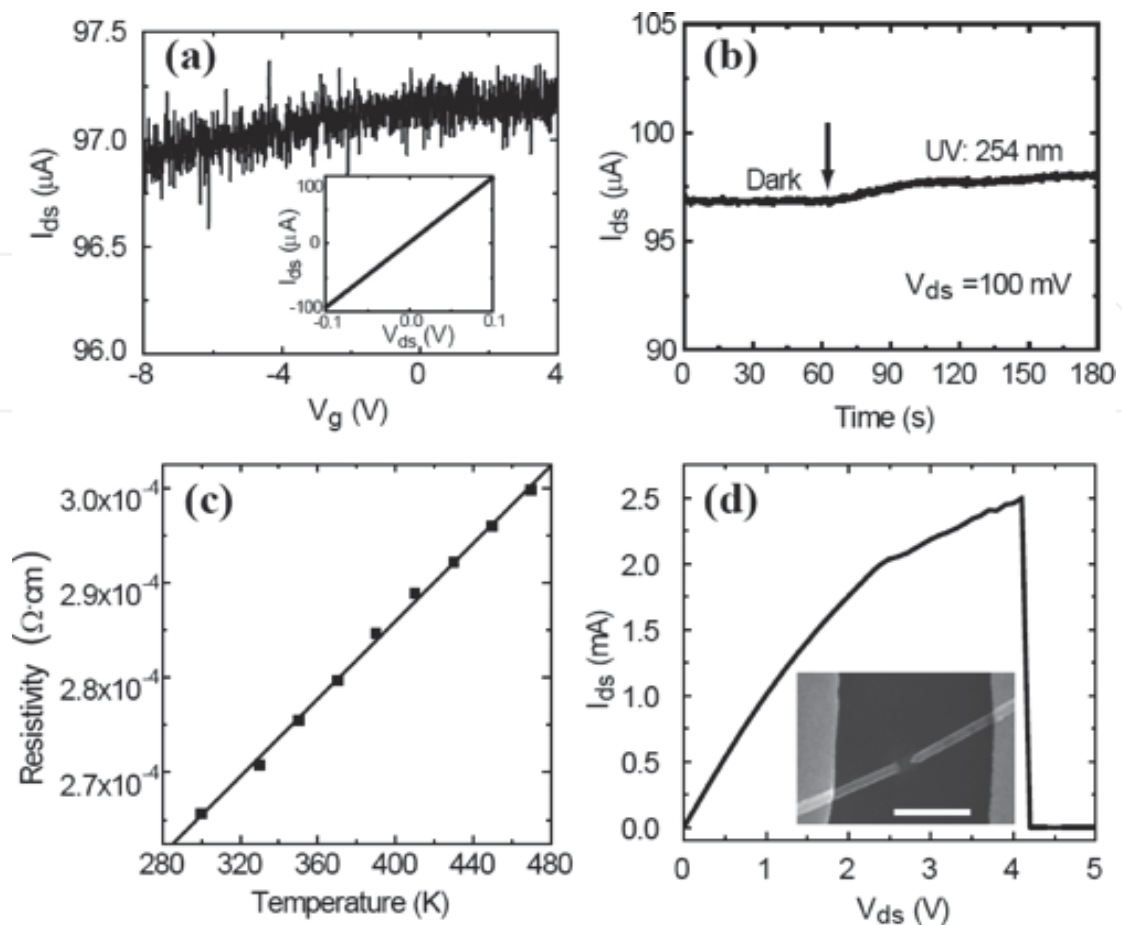
Fig. 5. Electrical characterization of a single ITO nanowire device. (a) Transfer curve (I_{ds}−V_g) of the ITO nanowire device at V_{ds}=100 mV. Inset, Ids−Vds curve of the device. The two-probe resistance of the device is ~1.05 kΩ. (b) UV response of the same device. (c) Temperature-dependent resistivity values of the ITO nanowire (300−470 K). The solid line is a linear fit. (d) I_{ds}−V_{ds} curve for the same ITO nanowire at large biases. The nanowire can carry a current of more than 2.5 mA before breaking down. Inset, SEM image of the failed ITO nanowire, showing that failure occurs in the middle of the nanowire. Scale bar: 500 nm.

Such high Sn doping levels will in fact render the ITO nanowires degenerately doped. Indeed, metal-like behaviors were observed in these ITO nanowire devices, as shown in Figure 5. Figure 5a shows the gate response curve of an ITO nanowire device with 90 nm lateral size and 3.2 μm channel length. The current Ids shows very little relative change as the gate voltage Vg is changed from −8 to 4 V. As a first-order estimation, the carrier density of the ITO nanowire can be calculated to be ~4.3 × 10^{20} cm^{-3} from the slope of the Ids−Vg curve. Such high carrier densities easily put the ITO nanowires in the degenerately doped regime. Assuming all Sn atoms are activated at room temperature, the Sn:In ratio can then be estimated to be 1.4:100, on the same order of the EDS estimations. Considering the simplicity of the model being used to calculate the carrier density and the small Sn signal used in the EDS estimations, such level of agreement is remarkable and verifies that a Sn-doping level of a few percent has been achieved in the ITO nanowires. The high doping level also explains the lack of UV response of these ITO nanowire devices (Figure 5b) and the insensitivity to the ambient environment. Contrary

to undoped In_2O_3 nanowires which are very sensitive to UV light due to photogeneration of carriers, the ITO nanowire device shows only ~1.0% change in conductance when illuminated by UV light, even though the photon energy of the applied UV source (254 nm, 4 W) is clearly above the band gap of ITO. This lack of UV response is a direct result of the high starting carrier concentration. The metallic behavior was further verified by temperature-dependence measurements (Figure 5c), in which the resistivity of the ITO nanowire increases linearly from $2.66×10^{-4}$ to $2.99×10^{-4}$ $\Omega\cdot cm$ as the temperature is increased from 300 to 470 K. This behavior agrees well with the expected linear resistivity−temperature relationship at high temperatures for a metal when scattering is dominated by electron−acoustic phonon scattering. Detailed temperature dependence studies on another device with room-temperature resistivity of $6.69×10^{-5}$ $\Omega\cdot cm$ show that the resistivity of the ITO nanowires over a wide temperature range (50−300 K) can be well described by the Block−Grüneisen formula, as expected for a metal or a degenerately doped semiconductor. Finally, these "metallic" ITO nanowires can also carry a very high current density due to the single-crystalline nature. As shown in Figure 5d, the ITO nanowire device can endure a current of 2.5 mA before failure, corresponding to a current density of $3.1 × 10^7$ A/cm^2.

3.2.2 Antimony -doped tin dioxide

Tin dioxide (SnO_2) represents an important metal oxide semiconductor that can be suitable for a range of applications through the incorporation of dopants, the electrical properties of SnO_2 nanowires as a function of antimony (Sb) doping were studied by Q. Wan [10]. Undoped, lightly (<0.5% Atomic mole ratio) and heavily (2–4%) Sb-doped SnO_2 nanowires were synthesized by a vapor-transport method via VLS mechanism under the same conditions. Figure.6 (a) shows a low-magnification transmission electron microscopy (TEM) image of the as-synthesized heavily Sb-doped SnO_2 nanowires. The catalyst nanoparticles are clearly visible on the tips of the SnO_2 nanowires, which confirm the VLS growth mechanisms. High-resolution TEM (HRTEM, Figure.6 (b)) confirms that the SnO_2 nanowires are single crystals with a tetragonal rutile structure.
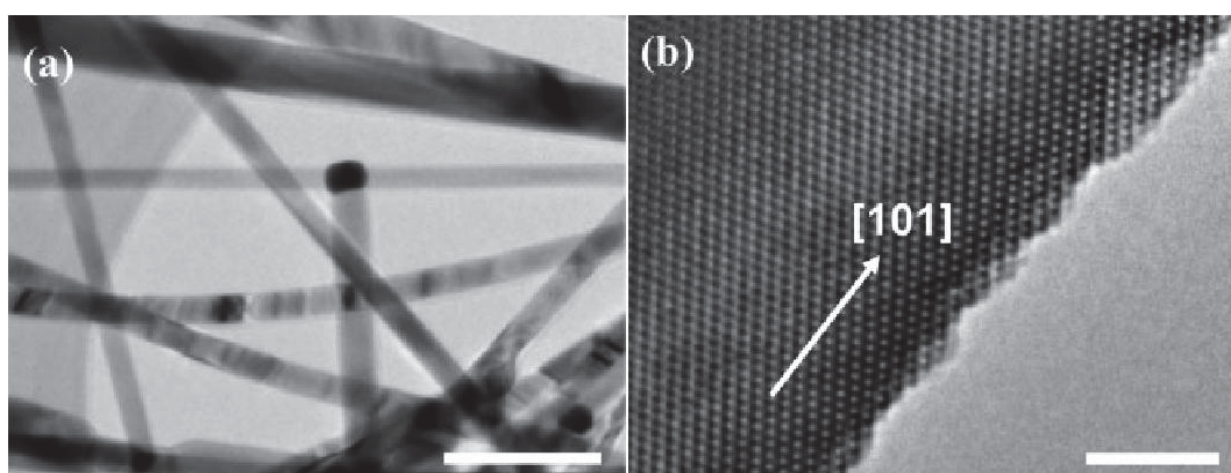

Fig. 6. (a) Low-magnification TEM image of degenerately Sb-doped SnO_2 nanowires. Scale bar: 100 nm. (b) HRTEM image of a single SnO_2 nanowire. Scale bar: 5 nm. (From ref. [10]).

Figure.7 (a) shows the current–voltage characteristics of an undoped SnO_2 nanowire device. A rectifying behavior (curve a) is normally observed in the air without illuminations, which indicates the formation of Schottky barriers at the metal/semiconductor interface. Upon illumination by UV light (254 nm), a linear current–voltage (ohmic-like) response (curve c) was observed along with a much higher current level. The ohmic-like behavior can be explained by enhanced electron tunneling at the metal/semiconductor interface due to an increase of the carrier density and the reduction of the depletion width upon illumination with above-bandgap photons, as reported for ZnO nanowire Schottky diodes [59-60]. Figure 7(b) shows the response of the device as a function of time (t) as the UV source was switched on and off. The current rapidly increases from 2 pA to 1mA upon UV illumination. The device can be reversibly switched between the low and high-conductance states with the response and recovery times estimated to be 1 s. The photocurrent sensitivity was estimated to be 5×10^5, a value much higher than that reported for undoped SnO_2 nanowire devices with ohmic contacts [49], due partly to the small dark current.
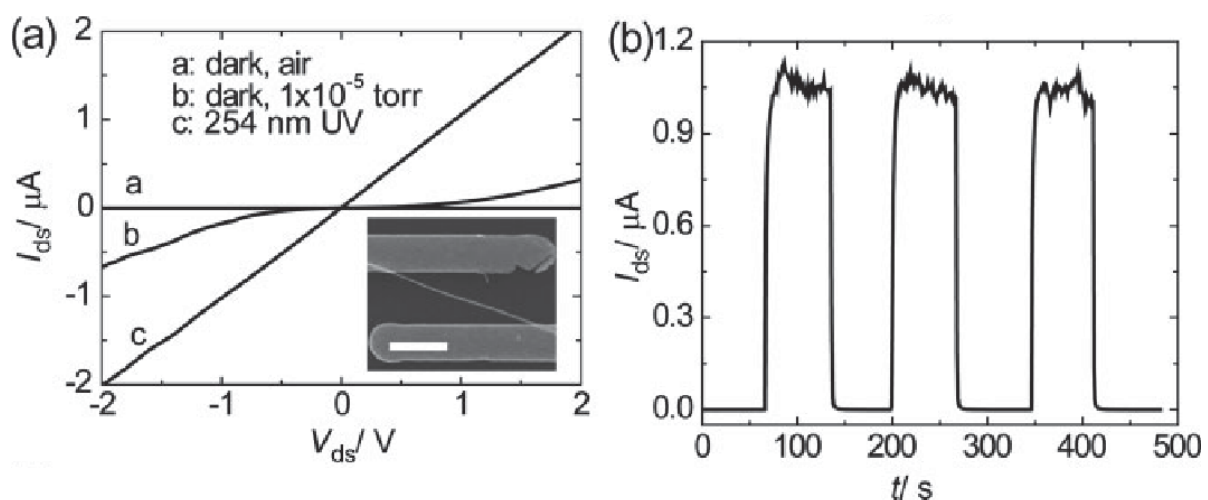

Fig. 7. Electrical properties of an undoped SnO_2 nanowire. (a) I_{ds}-V_{ds} curves of a nanowire device measured in the dark (curve a, in air and curve b, in vacuum) and exposed to 254-nm UV (curve c, in air). Inset: scanning electron microscopy (SEM) image of the SnO_2 nanowire device. Scale bar: 3mm. (b) Reversible switching of the nanowire device between low- and high-resistivity states as the UV light was turned on and off at different times t. The voltage bias on the nanowire was 1V (From Ref. [10]).

Form the above results, it could be concluded that the undoped SnO_2 nanowire devices show very poor transistor behavior in the air due to their high resistivity and the formation of Schottky contacts. The electrical performance of SnO_2 nanowires can be significantly improved by Sb doping. Figure 8 (a) shows typical I_{ds} -V_{ds} curves at different gate–source (Vgs) for a lightly Sb-doped SnO_2 nanowire configured as a field-effect transistor (FET) device. Linear behaviours in I_{ds} -V_{ds} curves are always observed for Sb-doped SnO_2 nanowire devices at low biases, which indicate low-resistance ohmic contacts between the nanowire channel and the Ti/Au electrodes. I_{ds}-V_{gs} curves obtained for the Sb-doped SnO_2 nanowire FET show that the device operates in the depletion mode as a result of the effective n-type doping with a transconductance (g) of 236 nS and an electron mobility of 550 cm²V⁻¹s⁻¹ at V_{ds} = 0.1 V. The on/off ratio and sub-threshold slope for the Sb-doped SnO_2 FET device are 1×10^5 and 0.17 V decade⁻¹ at Vds = 0.1 V, respectively. These excellent electrical properties confirm that the lightly doped SnO_2 nanowires are well-suited for transistor applications [54-55].
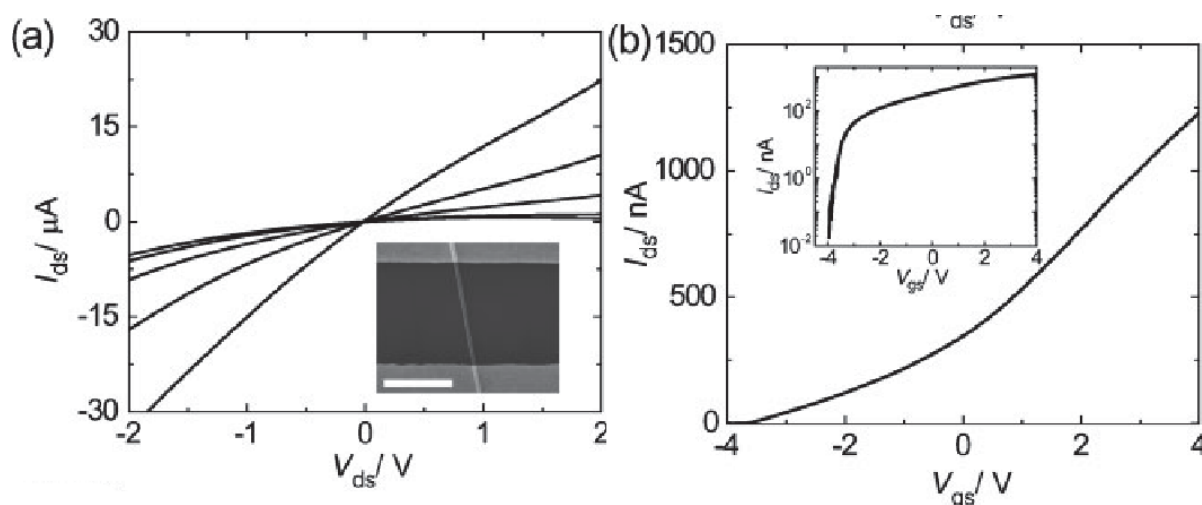
Fig. 8. Electrical properties of a lightly Sb-doped SnO_2 nanowire configured as a FET device. (a) Family of I_{ds} -V_{ds} curves at different gate–source Vgs. Vgs was varied from +4 to -4 V in steps of -2V and the device was measured in air at room temperature. Inset: SEM image of the device. Scale bar: 1.5mm. (b) Transfer (Ids -Vgs) curve of the same nanowire device at Vds =0.1 V. Inset: semilog plot of the Ids -Vgs curve (From Ref. [10]).
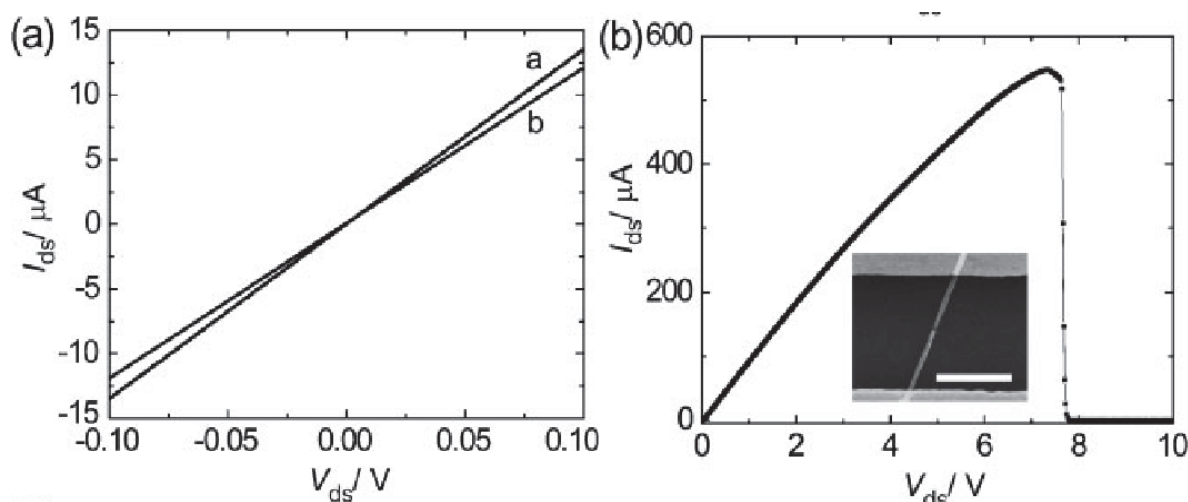

Fig. 9. (a) I_{ds} -V_{ds} characteristics of a SnO_2:Sb nanowire device measured in air without (curve b) and with (curve a) illumination by 254-nm UV light. (b) I_{ds} -V_{ds} curve recorded for the same SnO_2:Sb nanowire device, which shows the breakdown at very high current densities. The SnO_2:Sb nanowire can carry a current of more than 0.5 mA before breaking down. Inset: SEM image of the failed nanowire, which shows that failure occurs in the middle of the nanowire. Scale bar: 1 mm (From Ref.[10]).

The SnO_2 nanowires can be further doped to show metallic behavior by increasing the Sb:Sn ratio in the source during nanowire growth. The electrical properties of a degenerately (2–4 at%) Sb-doped SnO_2 (SnO_2:Sb) nanowire are shown in Figure 9 (a) with an estimated resistivity of $5.8 \times 10^{-4}\,\Omega$ cm in the dark. Due to the much higher carrier concentration, the SnO_2:Sb nanowires show a much smaller response (about 11.0%) to the same UV light compared to that for the undoped nanowires. As reported earlier [56], the SnO_2:Sb nanowires can also endure a high current density before failure. The failure current of 0.572 mA in Figure 9 (b) corresponds to a current density of $1.95 \times 10^{-7} A/cm^2$. The low resistivity

and high failure density in turn make the SnO_2:Sb nanowires desirable for applications in nanoscale interconnects and electron field emitters.

These results show that Sb doping has significant influences on the electrical properties of SnO_2 nanowires. Undoped SnO_2 nanowires are hardly conducting and form Schottky contacts with metal electrodes. The nanowire Schottky devices are suitable in UV photodetector applications. On the other hand, lightly Sb-doped SnO_2 nanowires are well-suited to high-mobility transistor applications. A further increase in the doping level will result in the degenerately Sb-doped SnO_2 nanowires that show metallic behaviors with resistivity as low as $5.8 \times 10^{-4} \Omega$ cm and failure-current density as high as $1.95 \times 10^7 A/cm^2$.

3.3 The optical properties of doped semiconducting oxide nanowires

Due to the wide gap of 3.37 eV and the large exciton binding energy of 60 meV, ZnO has been recognized as a promising photonic material in the blue-UV region [61]. ZnO has been widely used for its optoelectronic properties [62]. At the same time, the dopants can also strongly influence optical properties of the nanowires. Kouklin's group studied the optical properties of Cu-doped ZnO Nanowires [63]. The Cu dopants have been found to be both electrically and optically active within the nanowires, and more significantly are also able to act as visible-light photoconduction activators. Energy dispersive spectroscopy (EDS) measurements of the nanowires are shown in Figure.10 and point to the presence of Zn, O, and Cu (the Si signal arises from the substrate) in the nanowires. The EDS spectrum of nanowires grown by an analogous mechanism but outside the boat is presented in the inset of Figure.10. These results suggest that the incorporation of Cu is distance sensitive and stronger for samples placed in close proximity to the target (for the conditions used in this work). Owing to the very high temperatures (800°C) during the growth of the nanowires, doping has likely been achieved by two distinct routes: diffusion through sidewalls and/or direct deposition via solid–liquid interfaces present during VLS growth.
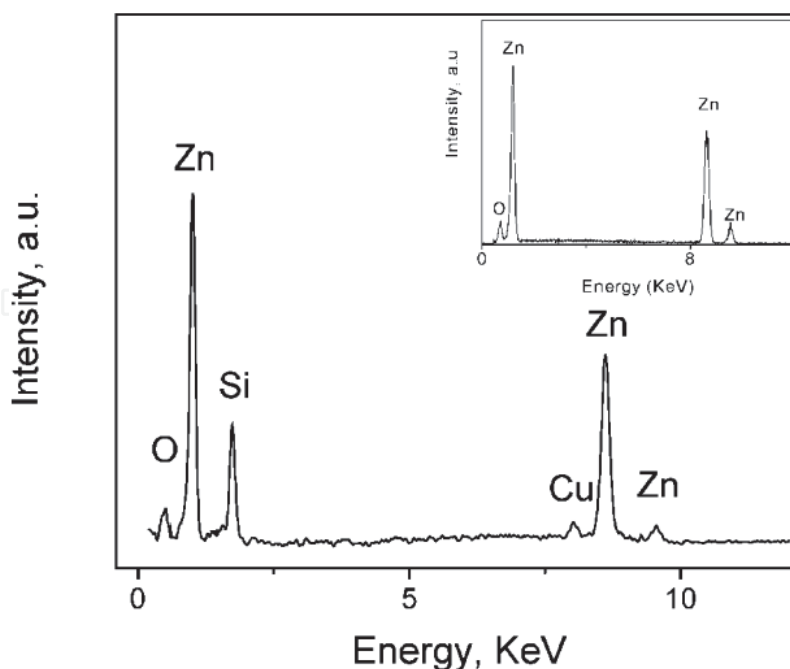

Fig. 10. EDS spectrum obtained for Cu:ZnO nanowires grown by VLS on top of a (111) Si substrate; the inset shows an EDS spectrum of ZnO nanowires grown on substrates located outside the boat (From Ref. [63]).

A typical PL spectrum is presented in Figure.11 and is clearly dominated by two peaks centered at 382 nm and 493 nm, referred to as free exciton and blue–green (BG) emission bands, respectively. A low-intensity shoulder peak at 455 nm has also been observed. The two main bands exhibit small red-shifts of 7 nm and 3 nm in their peak positions as compared to undoped samples (data not shown). Additionally, a two orders of magnitude increase in the ratio of BG to excitonic intensities of Cu:ZnO samples has been observed upon Cu doping. The appearance of a BG band and strong quenching of the exciton peak have been previously reported for thin films and nanowires of ZnO containing Cu impurities [64-65]. Therefore, the observed spectral changes upon doping can be primarily attributed to a drastic increase in the BG PL emission originating from the introduction of Cu centers.
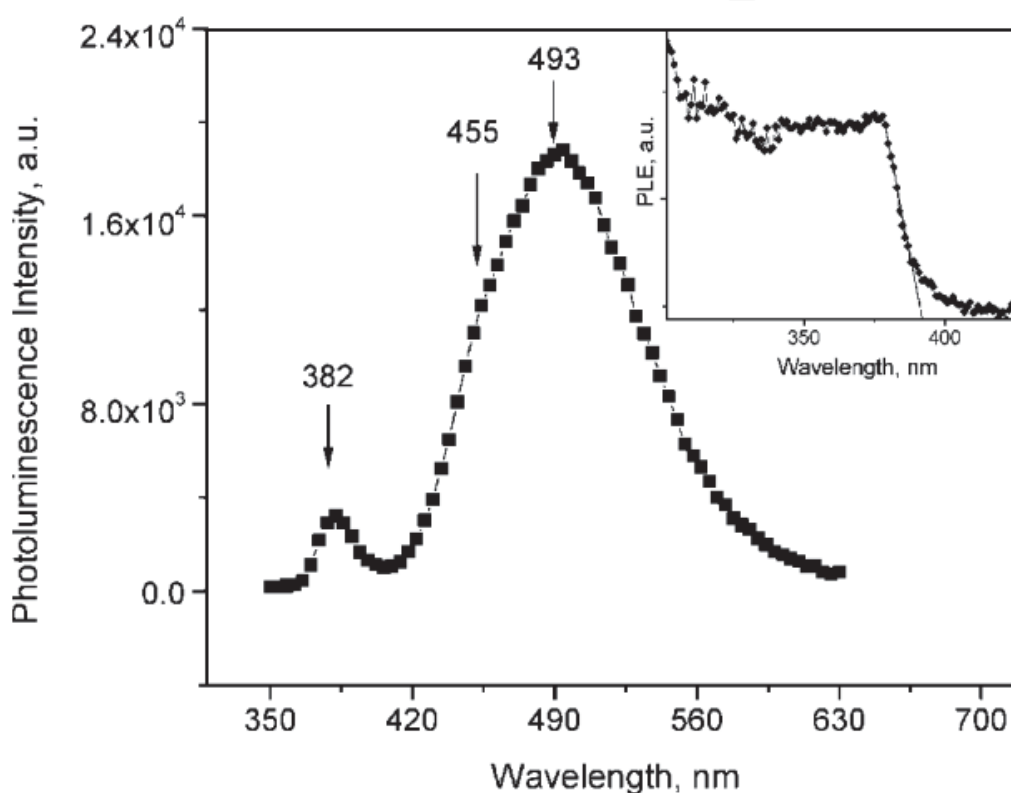

Fig. 11. RT micro PL spectrum of Cu:ZnO nanowires excited with a 325 nm light source. The inset displays the corresponding PLE spectrum with the emission monitored at 493 nm (From Ref. [63]).

PLE spectra have been obtained for Cu:ZnO nanowires at RT by monitoring their emission at 493 nm. The inset of Figure 11 shows the measured PLE data, clearly demonstrating the presence of a well-defined step in the emission intensity corresponding to an excitation wavelength close to 390 nm. The extrapolated intercept on the $\hbar\omega$-axis yields an effective bandgap of 3.17 eV, which is slightly red-shifted (by ca. 50meV) compared to that of pure ZnO nanowires. No light emission has been obtained for excitation energies less than E_{gap}, which is consistent with the previous results for Cu:ZnO materials. The studies presented here suggest the possibilities of engineering low-power nano-photodetectors and optical switches spanning multiple spectral ranges with improved gain characteristics by employing individual Cu-doped ZnO nanowires.

The effects of different doping level on the optical properties of doped ZnO nanowire need to be studied further. For example, the optical properties of S-doped ZnO nanowires were reported by Geng *et al* [66]. Figure.12 shows the results of the EDX measurements which were made on a different individual nanowire. The EDX pattern indicates that the nanowire is mainly composed of Zn and O with a small amount of S. S-doped ZnO nanowires with different content of sulfur have been obtained by changing the time of oxidation. Figures.12 (a), 12 (b), and 12 (c) correspond to 60, 90, and 100 min of oxidation time, respectively. When the time of oxygen stream lasted for 120 min, the pure ZnO nanowires have been obtained as shown in Figure.12 (d).
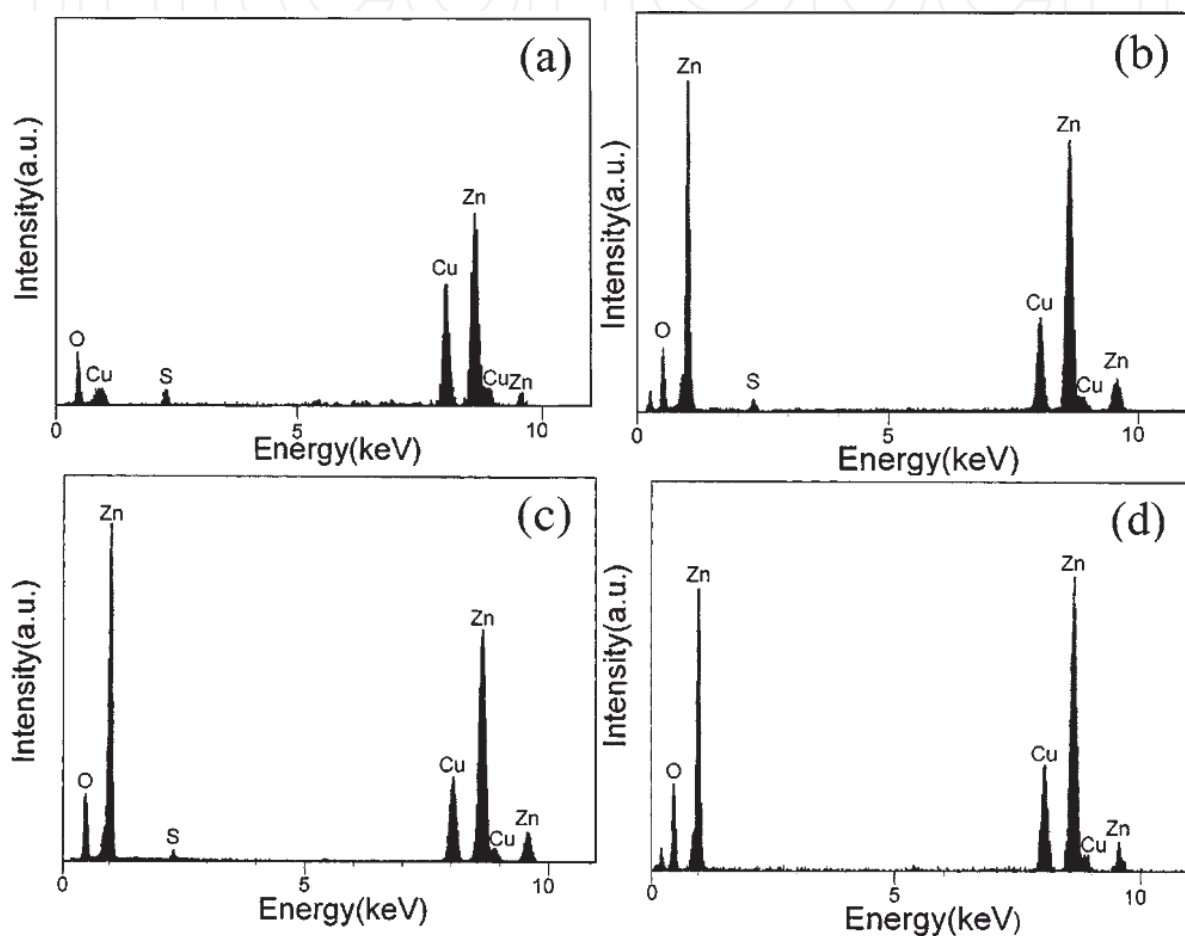

Fig. 12. EDX spectra of individual nanowire. Fig. 12 (a), 12 (b), 12 (c), and 12 (d) correspond to 60, 90, 100, and 120 min of oxidation time, and the corresponding content (atomic percent) of sulfur is 5.40%, 1.47%, 1.41%, and 0%, respectively (From Ref. [66]).

The room temperature photoluminescence spectra from ZnO nanowires and S-doped ZnO nanowires under the same experiment conditions are shown in Figure.13. Two luminescence bands have been observed for ZnO nanowire (curve d). One is an UV emission peak at 380 nm, which corresponds to the near band edge emission. The other luminescence band, a green light emission peak, was observed at 520 nm, which was attributed to the single ionized oxygen vacancy in ZnO. The PL spectra of S-doped ZnO nanowires with a different carrier concentration appear at an obviously blue shifted position. When ZnO is doped with S, the excess carriers supplied by the impurities to the conduction band contribute to increase the electrical conductivities of ZnO. Due to a small density of states of ZnO near the conduction-

band minimum, the conduction band edge is filled by excessive carriers provided by the impurities, leading to a blue shift of optical band-to-band transitions, known as the Burstein–Moss effect. It is worth noting that the blue shift increases with increasing carrier concentration, and the changes of PL intensity are observed at the same time. The UV emission peak weakens and the green light emission is enhanced. When S enters the ZnO crystal lattice, it introduces lattice distortion. Since S has a larger Bohr radius than O, it influences the energy structure of ZnO. The band gap broadens for the reasons mentioned above leads to the blue shift of the PL spectra and changes the intensity of near band edge emission. The probabilities of forming a new band structure deformation increases with the carrier concentration, which gives rise to some new defects, such as oxygen vacancies, therefore should result in the changes of the PL intensities of green light emission.
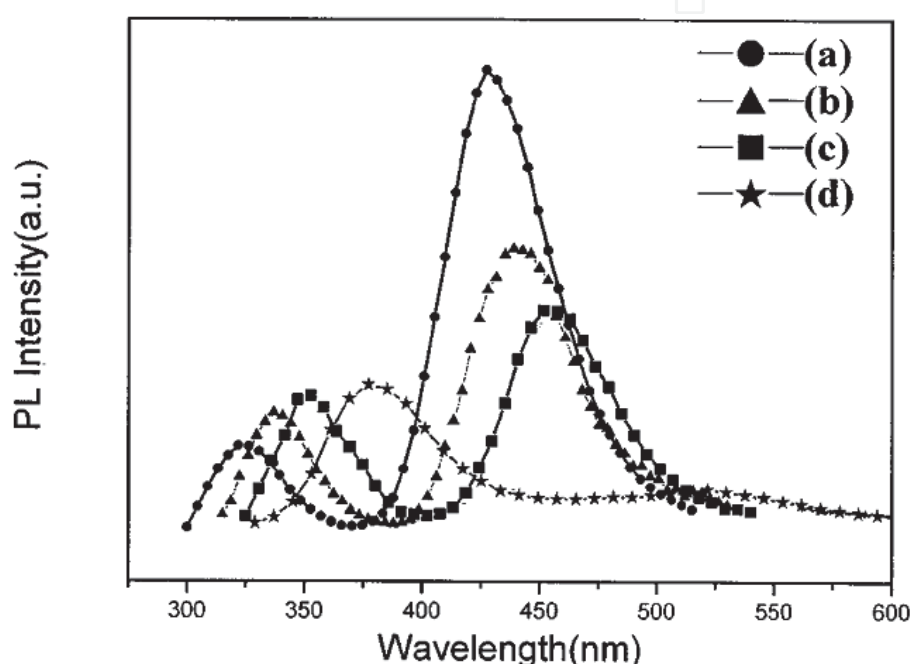

Fig. 13. The PL spectrum on a bulk quantity of nanowires measured at room temperature under 325 nm excitation. Curves (a), (b), (c), and (d) correspond to 60, 90, 100, and 120 min of oxidation time, and the corresponding content (atomic percent) of sulfur is 5.40%, 1.47%, 1.41%, and 0%, respectively (From Ref.[66]).

4. Applications of semiconducting oxide nanowires

4.1 Field-effect transistors based on semiconducting oxide nanowires

As one of the most functional components, field-effect transistors (FETs) using semiconducting oxide nanowires as active channels have been extensively investigated in the past few years [1-11]. A typical semiconducting oxide nanowire-based FET structure is shown in Fig. 14. In its simplest form, a semiconducting oxide nanowire is transferred onto a gate dielectric/gate electrode/substrate and is contacted with metallic source and drain electrodes. The nanowire and the gate electrode are capacitively coupled such that the application of a bias on the gate electrode induces charges in the nanowire. The voltage applied between the source and drain is referred to as the source-drain voltage, V_{DS}. For a given V_{DS}, the amount of current that flows through the nanowire from source to drain is a strong function of the gate voltage V_G. Since most of the oxide nanowires are n-type

semiconductor materials, the gate electric field can induce electrons to be mobile in the nanowire channel of the FETs when applying positive voltage to the gate electrode. Thus, the device is "ON". While, a decrease in nanowire channel conductance is experienced when applying negative voltage to the gate electrode. Thus, the device is "OFF". Up to now, various semiconducting oxide nanowires have been studied for the fabrication of FETs, including ZnO [1-6], In_2O_3 [7-9], SnO_2 [10-11], and so on. In this section, some typical works on the FETs built on semiconducting oxide nanowires are summarized.
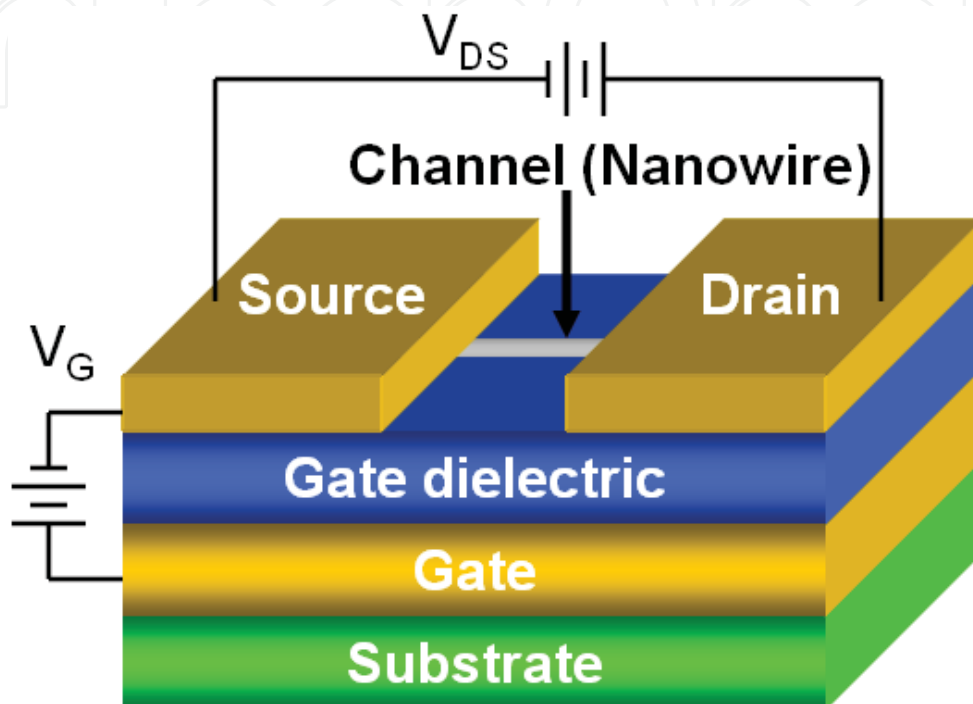

Fig. 14. Schematic image of the nanowire-based field-effect transistors

4.1.1 Device architecture of semiconducting oxide nanowire-based FETs

1. Back-gate FETs

Due to its fabrication simplicities, most of semiconducting oxide nanowire-based FETs are back-gated. The typical device fabrication processes are described as follows. Semiconducting oxide nanowires were synthesized by a variety of methods. Then, nanowires were transferred onto the degeneratively doped Si wafers coated with a layer of gate dielectric [2]. The source/drain electrodes were patterned by optical lithography and the metal contacts were deposited via electron beam evaporation. Figure 15 (a) shows a scanning electron microscope (SEM) image of a typical semiconducting oxide nanowire FETs. According to the cylinder-on-plate capacitance model, the back gate capacitance can be calculated using the relationship: $C_i = \dfrac{2\pi\varepsilon\varepsilon_0 L}{\ln(4h/d)}$.

Here L is the length of the nanowire device channel, ε_0 is the vacuum dielectric constant, h (nm) is the thickness of the gate dielectric layer, and d (nm) is the lateral size of the nanowire, ε is the relative dielectrics constant. The typical field-effect mobility of back-gate FETs is 10-100 cm²/Vs. And these devices shows a reasonable current ON/OFF ratio of 10^3~10^6. Figure.15 (b)

shows the output characteristic plot of the device. In general, the I_{DS} versus V_{DS} curves are linear at low bias, suggesting the ohmic contact at nanowire-electrode interface.
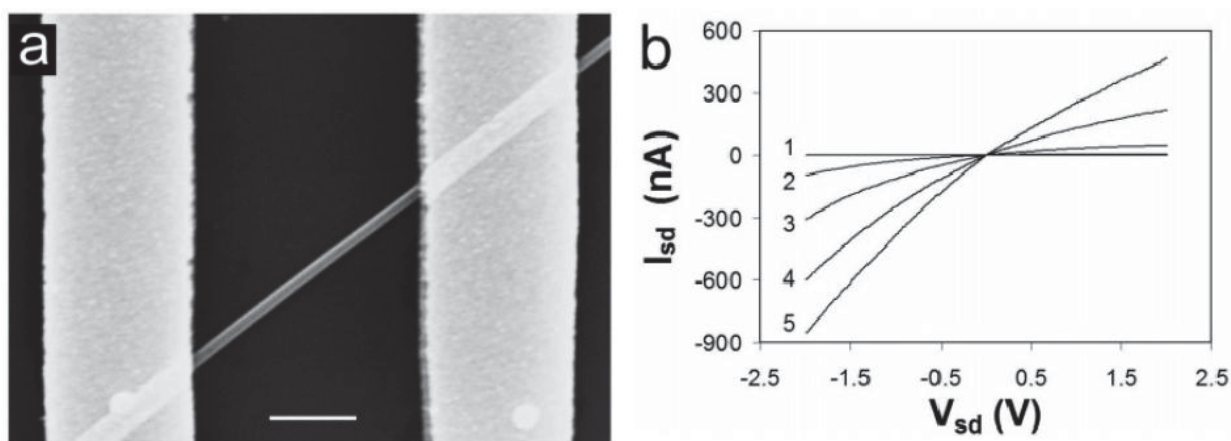

Fig. 15. (a) SEM image of a back-gated ZnO nanowire FET (scale bar: 1μm). (b) I_{DS} versus V_{DS} curves recorded at different gate voltages (From Ref. [2]).

2. Top-gate FETs

It is impossible to individually control each FET for the back-gated semiconducting oxide nanowire-based FETs, because heavily doped substrates are usually worked as the gate electrodes. Thus, top-gate nanowire FETs were developed. S. J. Pearton *et al* have reported single top-gate ZnO nanowire FET [3]. Figure 16 shows the SEM image of the top-gate nanowire FETs. The depletion-mode ZnO nanowire FET exhibits excellent pinch-off and saturation characteristics and a strong UV photo-response effect. A threshold voltage of ~-3 V and a maximum transconductance of 0.3 mS/mm were obtained. These devices look promising for the novel nanodevice applications requiring low leakage current.
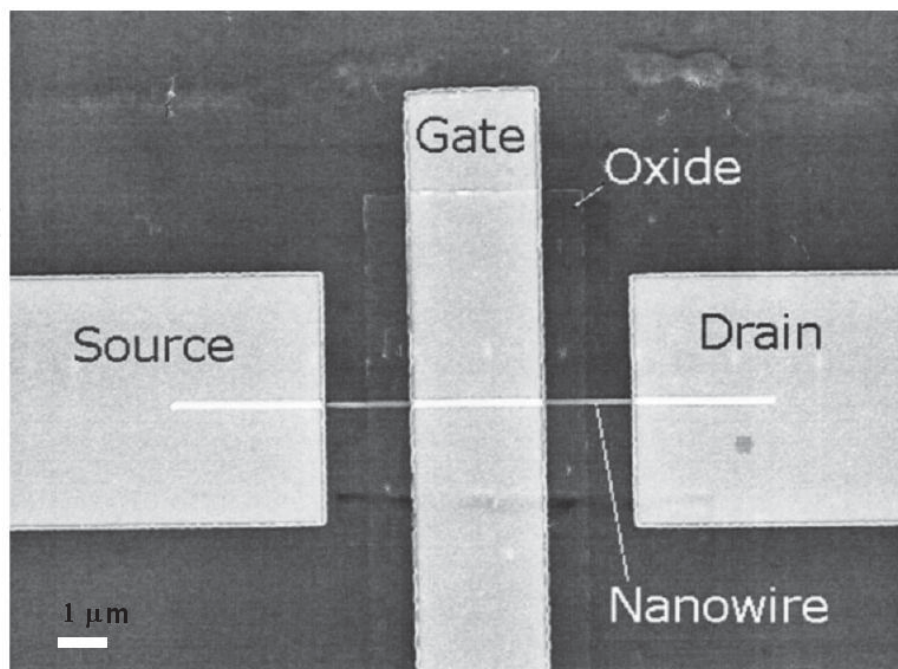

Fig. 16. SEM image of the top-gate nanowire FETs (From Ref. [3]).

3. Surround-gate FETs

As device dimensions continue to shrink into nanometer scale regime, fundamental physical limits and economic are likely to hinder further scaling according to Moore's law. New strategies including the usage of innovative device architectures are needed to extend the current capabilities. It is known that the fabrication of surround-gate FETs with Si nanowire channel was firstly achieved by the Lieber's group. In addition to the traditional back and top-gate FET, vertical surround-gate FETs was also achieved in semiconductor oxide nanowires by Hou T. Ng *et al*. The realization of a vertical surround-gate nanowire FETs takes the advantages of the vertical dimension unlike planar nanowire-based FETs and traditional metal-oxide-semiconductor (MOS) FETs [4]. Importantly, the device performance can be improved by applying this device architecture. Figure17 shows the fabrication processes of the vertical surround-gate FET. This fabrication method has allowed a lithography-free means of defining the vertical channel length and reduced the footprint of the devices since the source, drain and channel are stacked on top of each other vertically. The fabricated devices show a subthreshold swing of ~130 mV/decade and a large current ON/OFF ratio of larger than 10^5.
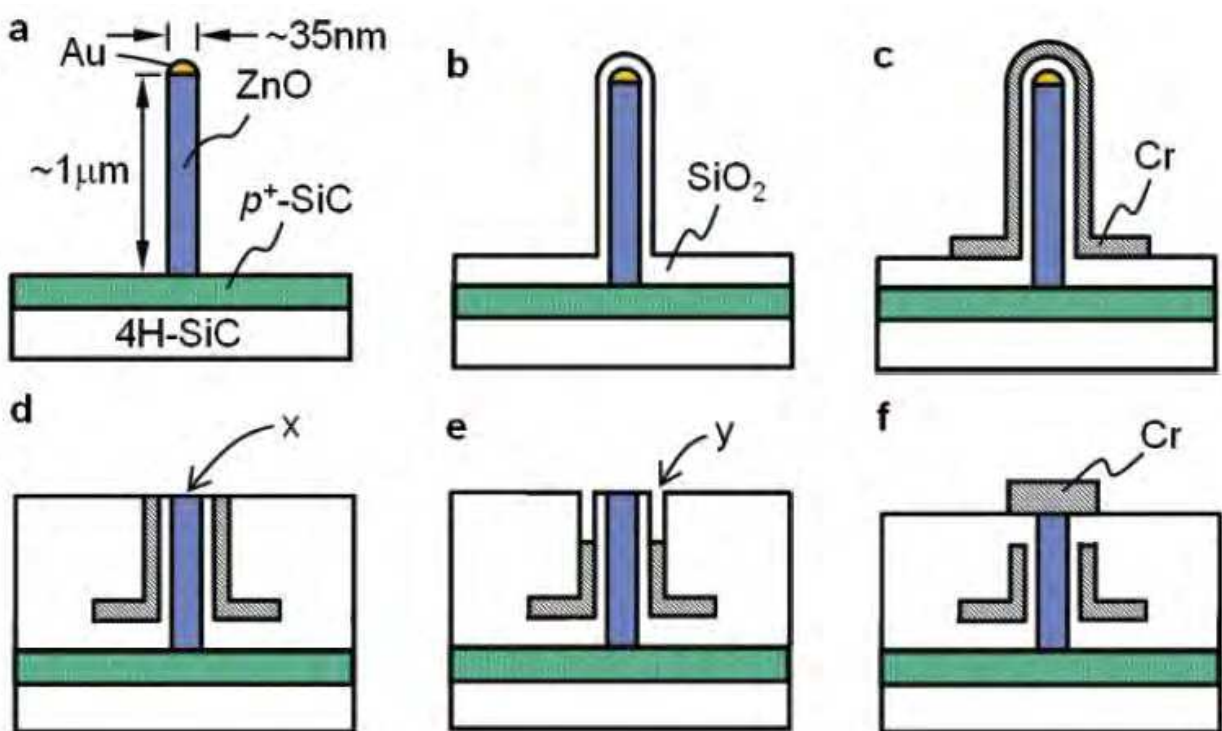

Fig. 17. The fabrication processes of the vertical surround-gate FET (From Ref. [4]).

4. Omega-shaped-gate FETs

Although surround-gate nanowire FETs are interesting and promising for novel nanodevice fabrications, there are only limited reports on the surround-gate nanowire FETs, due to the complexity associated with their fabrication processes. Theoretical simulations have predicted that omega-shaped-gate FETs should exhibit high device performances than surround-gate FETs, despite of their relatively simpler fabrication procedures. Thus, omega-shaped-gate device architectures were realized in semiconductor oxide nanowire-based FETs by Kihyun Keem *et al* [5]. Figure 18 shows the Schematic and top view SEM image of

omega-shaped-gate FET fabricated by the photolithographic process. About 80% of the surfaces of the nanowires coated with gate dielectric are covered with the metal gate to form omega-shaped-gate FETs. This device showed high performance with a mobility of ~ $30.2 cm^2/Vs$, a peak transconductance of 0.4 μS, and a high current ON/OFF ratio of 10^7. The observed improvements of electrical performances are mostly attributed to the omega-shaped-gate geometry and the passivation of the surface of the nanowires.
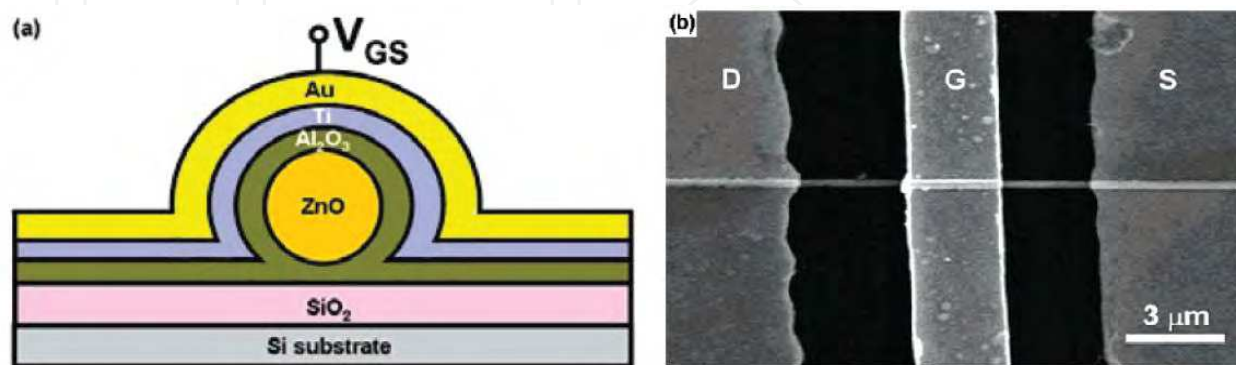

Fig. 18. (a) Schematic and (b) top view SEM image of omega-shaped-gate FET fabricated by the photolithographic process (From Ref. [5]).

4.1.2 Low-voltage semiconducting oxide nanowire-based FETs

Semiconducting oxides nanowire-based FETs are good building blocks for the functional nanodevices and are expected to lead to novel electronic and optoelectronic device applications [6]. To apply nanowires to various portable sensors and portable electronic device applications, there are several key challenges must be addressed [1]. In addition to the issues related to the integration of the nanowires into device structures with high yields and well-controlled contacts, development of compatible gate dielectrics with high specific capacitance and high gating efficiency is a significant issue in realizing device with low power consumption for portable applications. Some of the current strategies for increasing the gate specific capacitance have been reported, including using high *k* materials, reducing dielectric thickness and using solid electrolytes or ion gels as gate dielectrics.

1. High-k dielectrics gated nanowire-based FETs

The use of high-k gate dielectrics could result in the large capacitive coupling between the gate electrode and channel, therefore reducing the operating voltage of semiconductor oxide nanowire-based FETs. S. T. Lee group have demonstrated the fabrication of low-voltage Zn-doped In_2O_3 nanowire FETs with a SiN_x as a high-k dielectric [9]. The SiN_x dielectric was deposited by magnetron sputtering. The operating voltage of the FETs was reduced to as low as 2.0 V. The devices showed a high current ON/OFF ratio of ~10^6, a high ON-state current of 10^{-5} A, a small subthreshold swing of 120 mV/decade, and a near zero threshold voltage. Importantly, these devices show high reproducibility and stable performance. The high-performance nanowire-based FETs would enable the potential opportunities in the future multifunctional nanodevice applications.

2. Self-assembled organic nanodielectrics gated nanowire-based FETs

Most of the reported semiconductor oxide nanowires-based FETs have utilized gate dielectrics including thermally grown oxide layer and sputtering or chemical vapor deposited dielectric films. However, these gate dielectrics have limitations associated with

high temperature processing. It is not suitable for low-power flexible electronic applications. Sanghyun Ju *et al* have reported that self-assembled organic nanodielectric has been used as the gate dielectric for individual ZnO nanowire FETs fabrications [1]. Figure 19 (a) shows the cross-sectional view of the self-assembled organic nanodielectric gated ZnO nanowire FET device structure. The self-assembled organic nanodielectric films used in their studies consist of layer-by-layer organic monolayers. Such dielectrics exhibit excellent insulating properties with a large specific capacitance of 0.18 $\mu F/cm^2$ and a low leakage current density of 10^{-8} A/cm^2. Figure 19 (b) and (c) show the output and transfer characteristic curves of the ZnO nanowire FETs with a self-assembled organic nanodielectrics. The fabricated device display excellent I_{DS} saturation at V_{DS} of 0.5 V, a threshold voltage of -0.4 V, a carrier mobility of 196 cm^2/Vs, a current ON/OFF ratio of 10^4, and a subthreshold slope of 400 mV/decade. The operating voltage of these devices is as low as 2.0 V. These results indicate that self-assembled organic nanodielectric gated ZnO nanowire FETs are promising for future flexible display and logic technologies.
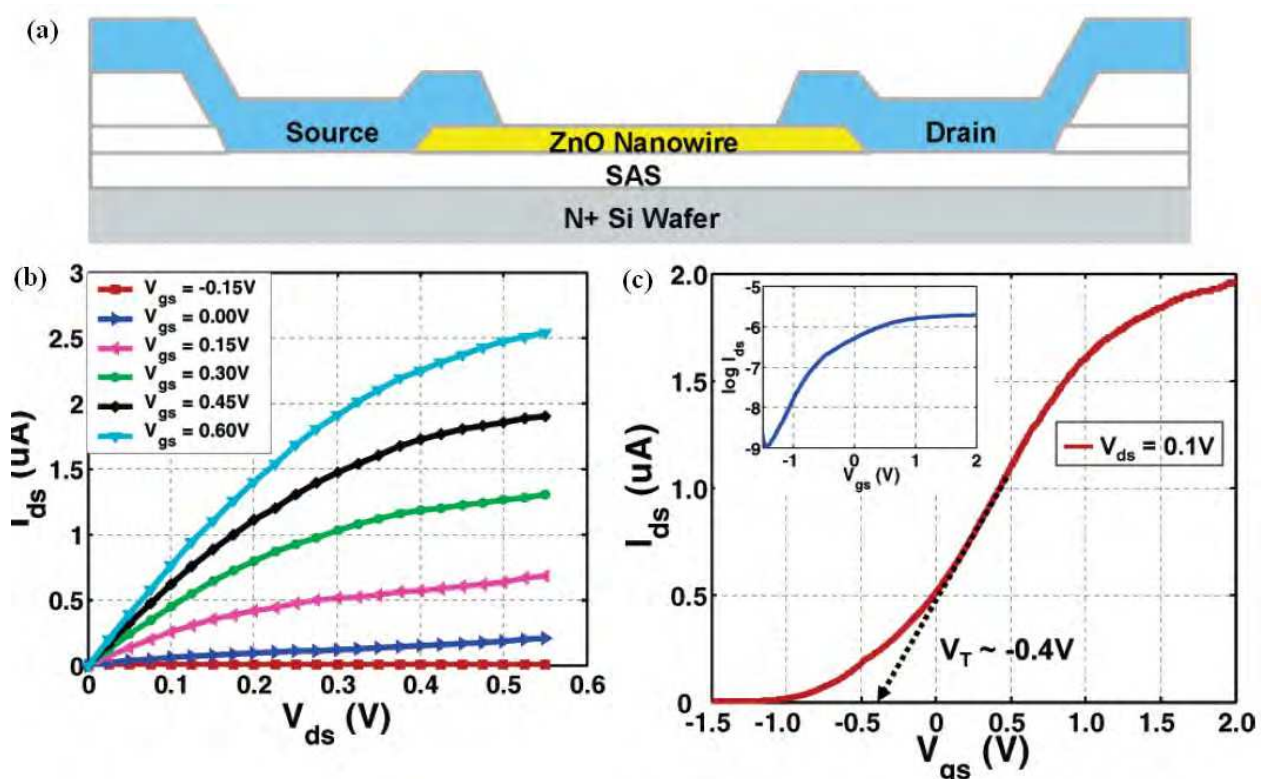

Fig. 19. (a) Cross-sectional view of the self-assembled organic nanodielectric gated ZnO nanowire FET device structure. (b) Output and (c) transfer characteristic curves of the ZnO nanowire FET with a self-assembled organic nanodielectric (From Ref. [1]).

3. Solid-electrolyte gated nanowire-based FETs

Another simple alternative for achieving low operating voltage is to exploit solid-electrolyte or ion gels as gate dielectrics associated with a large electric-double-layer (EDL) capacitance resulting from the short Debye lengths of a few nanometers. More importantly, these dielectrics gating eliminates hysteresis and provides a simple yet versatile method of studying fundamental electron transport in semiconductor oxide nanowire-based devices. Jia Sun *et al* have reported the fabrication of microporous SiO_2 solid-electrolyte gated low-

voltage SnO_2 nanowire FETs by nickel mask method [11]. The operating voltage is found to be as low as 1.5 V due to the extremely large specific capacitance (~ 2 $\mu F/cm^2$) related to the mobile ion-induced electric-double-layer effect.
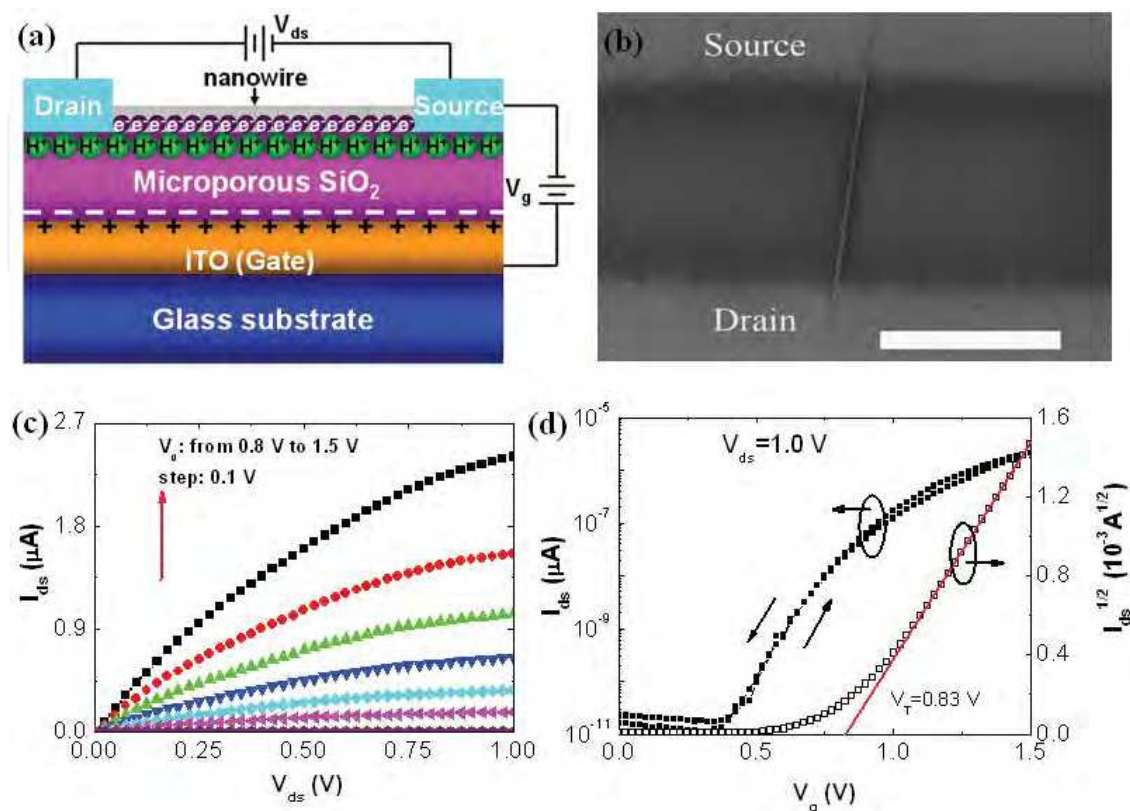

Fig. 20. (a) A schematic picture of the low-voltage operation of microporous SiO2 solid-electrolyte gated SnO_2 nanowire FETs. (b) A low-magnification SEM micrograph of the fabricated device. (c) Output and (d) transfer characteristic curves of the SnO_2 nanowire FET with a microporous SiO_2 solid-electrolyte gate dielectric (From Ref. [11]).

Figure 20 (a) shows the schematic diagram of the low-voltage operation mechanism of the SnO_2 nanowire FETs. When a positive gate voltage is applied, protons are drifted toward the SiO_2/SnO_2 nanowire channel interface where they accumulate over a Debye length L_D, and the positive charges induces an image charge and opposite sign in the SnO_2 nanowire channel layer, which is similar to the case of the EDL formation in organic transistors gated by ion gel or polyelectrolyte. Figure 20 (b) shows a SEM image of SnO_2 nanowire FET. Figure 20 (c) and (d) shows the output and transfer characteristic curve of the microporous SiO_2 solid-electrolyte gated SnO_2 nanowire FET. The field-effect mobility, current on/off ratio and sub-threshold swing are estimated to be 175 cm^2/Vs, 10^5, and 116 mV/decade, respectively. We believe that such high-performance low-voltage SnO_2 nanowire transistors hold promise for novel device applications, such as portable ion-sensitive sensors.

4.1.3 Transparent semiconducting oxide nanowire-based FETs
Transparent electronics is a technology-in-a-hurry and its aim is to realize invisible electronic circuits in which transparent transistors are the most fundamental functional component. To achieve this objective and satisfy multifunctional applications in our daily

life, the ideal transparent electronic devices must achieve high optical transparency and be compatible with diverse low-cost substrates. Traditional poly-silicon and amorphous-silicon devices as well as the circuits are widely used to fabricate the commercial display. However, their lack of transparency limits their utilities in transparent electronics. Transparent oxide nanowires with wide band gap could meet the above-mentioned requirements. Recently, some researchers have reported transparent transistors fabricated with ZnO, SnO_2 and In_2O_3 nanowires. David B. Janes group has reported the fabrication of fully transparent In_2O_3 and ZnO nanowire FETs on both glass and flexible plastic substrates [7]. Figure 21 shows the optical and electrical characteristics of fully transparent nanowires FETs. These devices exhibit high-performance n-type transistor characteristics with ~ 82% optical transparency. Fully transparent nanowire FETs are also attractive as pixel-switching and driving transistors in active-matrix organic light-emitting diode displays. The same group has firstly reported the demonstration of active-matrix light-emitting diode displays driven by the nanowire FETs and shows that such displays can be optically transparent. These results indicate that nanowire FETs devices strategies are promising for windshield displays, head-mounted displays, transparent screen monitors, mobile phones, and handheld personal computer.
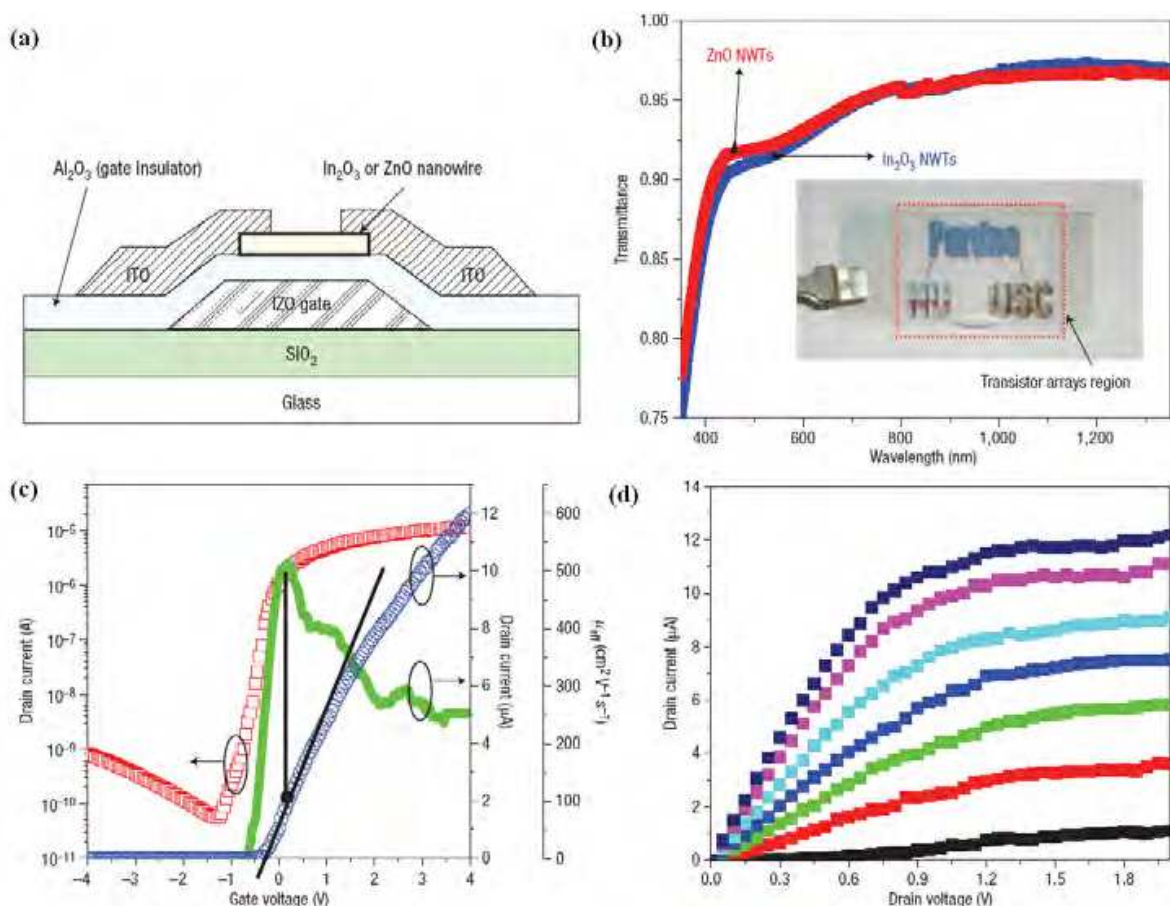

Fig. 21. (a) A schematic picture of fully transparent nanowire FETs. (b) Optical transmission spectra through entire nanowire FET sturctures. (c) Transfer and (d) output characteristic curves of the fully transparent nanowire FET (From Ref. [7]).
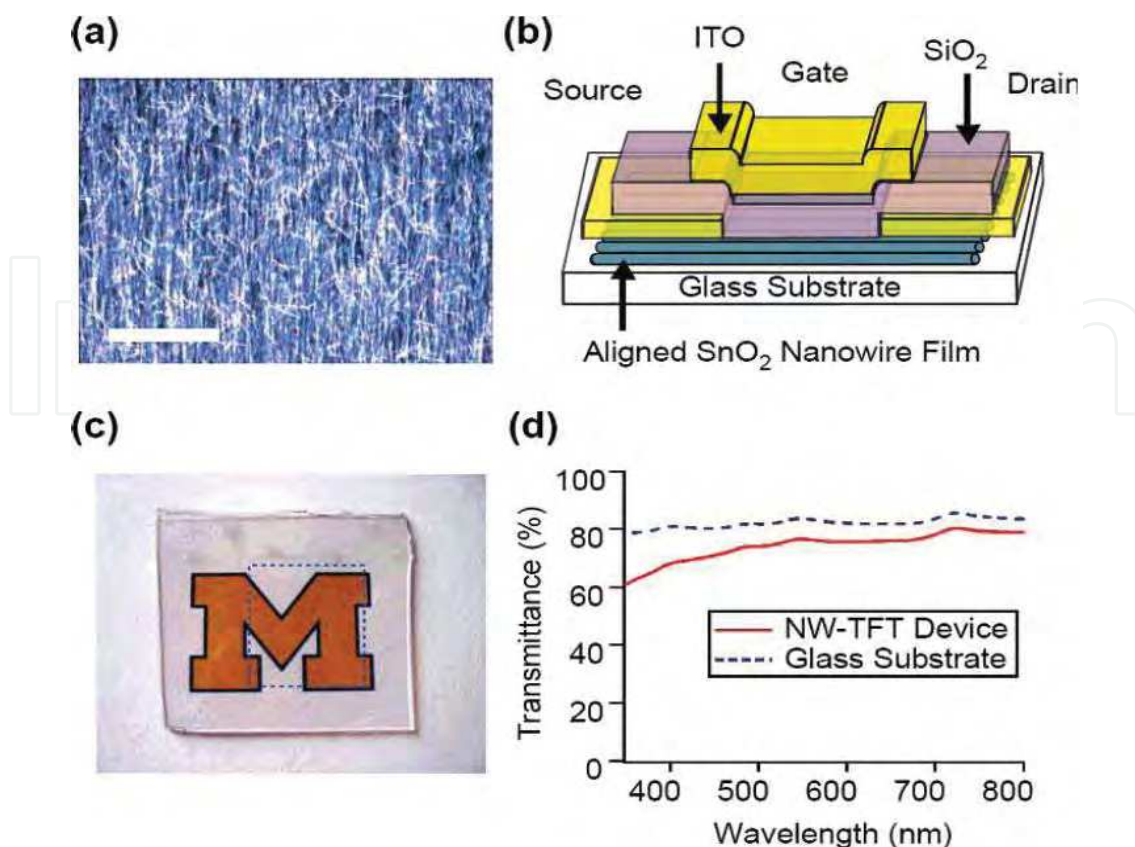
Fig. 22. (a) Dark-field optical microscope image of a SnO_2 nanowires films obtained through the physical transfer method. Scale bar: 20 µm. (b) Schematic of the transparent SnO_2 nanowire thin-film transistor device. (c) Digital photograph of SnO_2 nanowire thin-film transistor on glass. (d) Optical transmittance spectrum of the SnO_2 nanowire thin-film transistor device array (From Ref. [10]).

Semiconducting oxide nanowires have been used as interesting materials for the fabrication of high-performance transistors with electronic performance comparable to and in some cases exceeding that of single-crystal materials. A new concept of nanowire thin-film transistors has been proposed using oriented nanowire thin films as semiconductor channels. One of the key advantages of the nanowire thin-film transistors approaches compared to conventional thin-film transistor techniques is the clear separation of the device fabrication stage from the material growth stage. Therefore, it is no longer needed to concern with compatibilities with device substrates during growth. Wei Lu *et al* have fabricated fully transparent nanowire thin-film transistors based on lightly Ta-doped SnO_2 nanowires [10]. The nanowires-based devices exhibit uniform characteristics with average field-effect mobilities exceeding 100 cm²/Vs. As shown in Figure 22, prototype nanowires thin-film transistors devices on glass substrates show excellent optical transparency and transistor performance. They found that fully transparent nanowires thin-film transistors exhibit similar high-mobilities even with low nanowire coverages.

At last, Table 2 summarizes the performance parameters of different doped and undoped semiconducting oxide nanowires based transparent FETs. We believe that these high-performance transparent nanowires FETs are promising for a broad range of existing applications from flat-panel displays to image sensor arrays and enable a whole new range of flexible, wearable, or disposable electronics.

Channel materials	Gate dielectric	Operation voltage (V)	Subthreshold swing (V/dec)	Mobility (cm^2/Vs)	On/off ratio	Ref
ZnO nanowires	18 nm/Al$_2$O$_3$	4	0.3	70~96	10^6	30
In$_2$O$_3$ nanowires	18 nm/Al$_2$O$_3$	4	0.16	300~514	10^6	30
In$_2$O$_3$ nanowires	22 nm/self-assembled nanodielectric	4	0.25	258	10^5	7
Ta-doped SnO$_2$ nanowires	75 nm/SiO$_2$	10	0.312	179	10^5	39
Zn-doped In$_2$O$_3$ nanowires	150 nm/SiN$_x$	2	0.12	631	10^6	35
As-doped In$_2$O$_3$ nanowires	50 nm/Al$_2$O$_3$	5	0.088	1490	5.7×10^6	32
Sb-doped SnO$_2$ NW	4.0 μm/microporous SiO$_2$ solid-electrolyte	1.5	0.116	175	10^5	41

Table 2. The performance parameters summary of different doped and undoped semiconductor oxide nanowire based transparent FETs.

4.2 Sensors based on semiconducting oxide nanowires

Solid-state sensors play an important role in medical diagnosis, environmental monitoring, chemical process controlling, personal safety and national security. There is a strong interest in the developments of high-performance sensors with high sensitivities, high selectivities and low detection limits. Semiconducting oxides have been known as good sensing materials due to their low cost and high compatibilities with microelectronic processing. In recent years, semiconducting oxide naowires have been attracted much attention due to their great potential applications. The novel properties of semiconducting oxide nanowires, associated with a large surface-to-volume ratio, finite or quantum size effects and a Debye length comparable to their dimensions, offer the basis for the exploration of new and interesting phenomena. The extremely large surface-to-volume ratio makes their electrical properties more sensitive to species. Superior stabilities of semiconducting oxide nanowires based sensors can be obtained duo to the high crystallinity. Up to now, various sensors have been already reported based on semiconducting oxide nanowires, including gas sensors, biosensors, and so on. Table 3 summarizes some typical sensors based on semiconducting oxide nanowires. These sensors have good response and recover characteristics. As one can see, the most widely studied substances are ZnO, SnO$_2$ and In$_2$O$_3$, probably due to their relatively simple synthesis and good sensitivities to species. In this section, we present a comprehensive perspective on research efforts made on these kinds of sensors based on semiconducting oxide nanowires. The fabrication and testing as well as the device performances of these sensors are outlined.

Types of sensor	Materials	Target	Detection limit	Response time	Ref.
Gas sensors	In_2O_3 nanowires	NO_2	5 ppb	1000 s	15
	ZnO nanowires	Ethanol	1 ppm (300°C)	10 s	12
	ZnO nanowires	NO_2	0.5 ppm (225°C)	24 s	14
	SnO_2 nanowires	Acetone	20 ppm (290°C)	7 s	67
	SnO_2 nanowires	Ethanol	0.5 ppm (300°C)	4 s	18
	In_2O_3 nanowires	NO_2	1 ppm (250°C)	20 s	73
	CuO nanowires	CO	5 ppm (room temperature)	10 s	68
	TeO_2 nanowires	NO_2 NH_3 H_2S	10 ppm (26°C) 100 ppm (26°C) 50 ppm (26°C)	10 min	69
	Single Zn-doped In_2O_3 nanowire	CO	2 ppm (room temperature)	20 s	70
	Single ZnO nanowire	H_2	500 ppm (room temperature)	55 s	72
Biosensnors	Single ZnO nanowire	streptavidin	2.5 nM	Not available	71
	Single ZnO nanowire	hemoglobin	2 fg/mL (negatively charged)	< 1s	20
	ZnO nanowires	Glucose	1 μM	10 s	16
Other sensors	Single SnO_2 nanowire	Humidity	30 % relative humidity (30°C)	120-170 s	19
	Single ZnO nanowire	UV	1.5 mW/cm²	Less than 1 s	21
	Single ZnO nanowire	Strain	0.2 % strain	Less than 1 s	17

Table 3. Typical sensors based on semiconducting oxide nanowires.

4.2.1 Gas sensors based on semiconducting oxide nanowires

Up to now, semiconducting oxide nanowires based gas sensors are usually fabricated through resistors or FETs. These sensors are based on resistance changes caused by the exposure of the sensor surface to a target species. Chemisorbed gas molecules on a semiconducting oxide nanowires surface withdraw or donate electrons to the conduction channel, giving rise to a conductance, which is the fundamental working principle of these sensors. For the type of sensors based on resistors, the semiconducting oxide nanowire film is contacted with pairs of metal electrodes on a substrate of a ceramic tube. For the type of sensors based on FETs, a single or multiple nanowires bridge source and drain electrode on a substrate covered with gate insulator/gate electrode. The major advantages of these types of sensors are easy fabrication process, low cost and easy integration with heat transducers.

1. Semiconducting oxide nanowires gas sensors based on resistors

Wan *and co-workers* have demonstrated the fabrication of ethanol sensors based on ZnO nanowires by microelectromechanial system technologies. ZnO nanowires were ultrasonic dispersed in ethanol for 30 min and dried by an infrared light on a silicon-based membrane

embedded with Pt interdigitated electrodes and a heater [12]. Figure 23 (a) shows the top-view SEM image of the fabricated sensors. Figure 23 (b) shows the sensing properties of ZnO nanowires upon exposure to 1-200 ppm ethanol in dry air at 300 °C working temperatures. The sensitivities at 200 ppm ethanol exposure is estimated to be 47, and at 1 ppm ethanol exposure to be 1.9. The response and recovery is relatively quick, which is desirable for practical application.
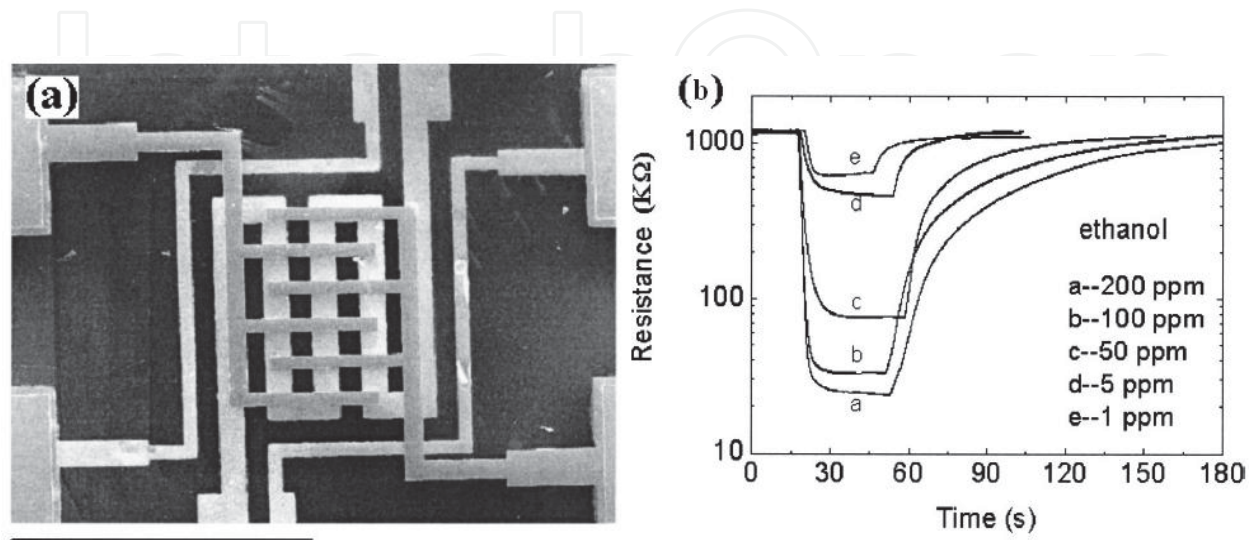

Fig. 23. (a) Top-view SEM image of the fabricated substrate embedded with Pt interdigitating electrodes and Pt heater (scale bar: 1mm). (b) Response and recovery characteristics of ZnO nanowires upon exposure to ethanol with a concentration of 1-200 ppm at 300°C (From Ref. [12]).

Recently, Wan and co-workers proposed an excellent performance of ethanol sensors based on the branched SnO_2 nanowire films [18]. The metallic backbones of Sb-doped SnO_2 nanowires dramatically reduced the resistance and the branched structure offered more pathways for electrical conductions in comparison with pure SnO_2 nanowire films, thus significantly reducing the detectable limits of ethanol to sub-ppm at 300 °C. These results indicate that semiconducting oxide nanowires can be used as the sensing materials for fabricating highly sensitive gas sensors.

Ahn *and co-workers* have fabricated novel ZnO nanowire gas sensors by a simple and efficient fabrication process and the gas-sensing capability is demonstrated for NO_2 gas [14]. Figure 24 (a) and (b) show a schematic illustration and SEM images of the fabricated sensors. The ZnO nanowires were synthesized and bridged the gap between two prepatterned Au catalysts. From the SEM image, we can see that the network-structured ZnO nanowires are floated on the SiO_2/Si substrate. The device structure proposed is very simple and efficient, because the electrical contacts to the nanowires are self-assembled during the synthesis of them. A good Ohmic behavior was obtained, which is important to the sensing properties because the sensitivities of a gas sensor can be maximized when the metal-semiconductor junction is Ohmic or has a negligible junction resistance. As shown in Figure 24 (c), the sensor displayed the fast responses and recovery behaviors with a maximum sensitivity to NO_2 gas at 225 °C. The response and recovery times are 24 s and 12 s for 0.5 ppm NO_2 gas.
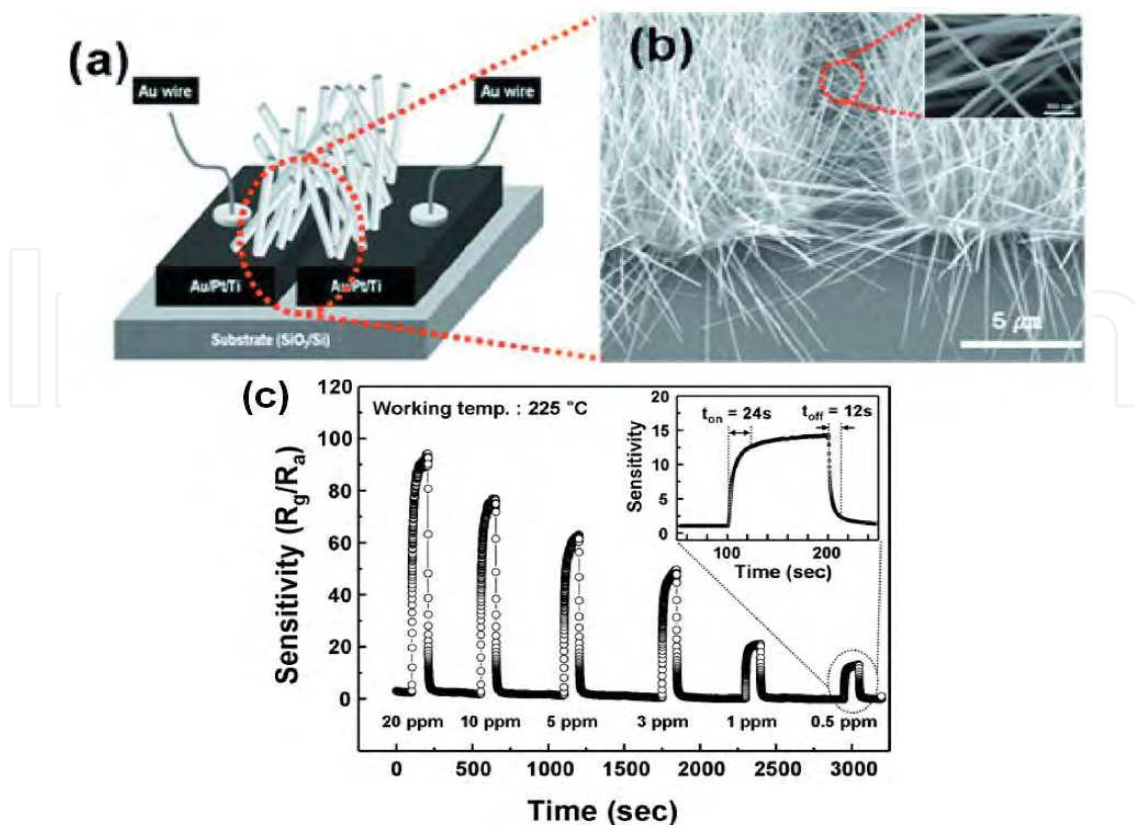
Fig. 24. (a) A schematic illustration and (b) SEM images for the network-structured ZnO nanowire floated SiO$_2$/Si substrate. (c) Gas sensitivity curves of the network-structured ZnO-nanowire gas sensor under exposure to 20, 10, 5, 3, 1, and 0.5 ppm NO2 gas at the measurement temperature of 225 °C (From Ref. [14]).

2. Semiconducting oxide nanowires gas sensors based on FET devices

The FET device configurations used for sensors can not only facilitate the monitoring of conductance change, but also utilize a transverse electric field to modulate the chemical sensing behaviors of the nanowires. Fan *and co-workers* have reported that n-type single ZnO nanowire FETs are implemented as chemical gas sensors for the detection of NO$_2$, NH$_3$, CO and O$_2$ [13]. Single-crystalline ZnO nanowires were synthesized via a vapor trapping chemical vapor deposition method. The as-synthesized samples were suspended in alcohol and deposited onto p^{++}-Si substrates capped with a SiO$_2$ insulator. Photolithography or electron beam lithography was used to define source and drain electrode patterns. Figure 25 illustrates an atomic force microscopy image of a ZnO nanowire FET combined with the schematic of the measurement circuit.

Zhou *and co-workers* have firstly demonstrated room-temperature detection of NO$_2$ down to ppb levels using single and multiple In$_2$O$_3$ nanowires FET. In$_2$O$_3$ nanowires with diameters of ~ 10 nm and lengths of ~ 5 μm were synthesized by the laser ablation method [15]. The single or multiple In$_2$O$_3$ nanowires FET followed the traditional micro-fabrication technology. The conductance of In$_2$O$_3$ nanowires is directly related to the carrier concentration which can be altered by the adsorbed NO$_2$ molecules due to their strong electron withdrawing capabilities, therefore the NO$_2$ sensing is expected. Single In$_2$O$_3$ nanowire FETs based sensors displayed high NO$_2$ sensitivity down to 20 ppb level. As shown in Figure 26, the multi-nanowire sensors showed an even lower detection limit of 5

ppb, as compared to the 20 ppb limit of single nanowire sensors. They attribute this improved sensitivity to the formation of nanowire/nanowire junctions between the metal electrodes. Such junctions, when exposed to NO_2, should form a depleted layer around the intersection and thus block the electron flow in a way more prominent than the surface depletion of single nanowires with metal contacts. These high-performance sensors are promising for a new generation of NO_2 sensors in terms of their low detection limits to ppb levels and great simplicities in the device fabrications.
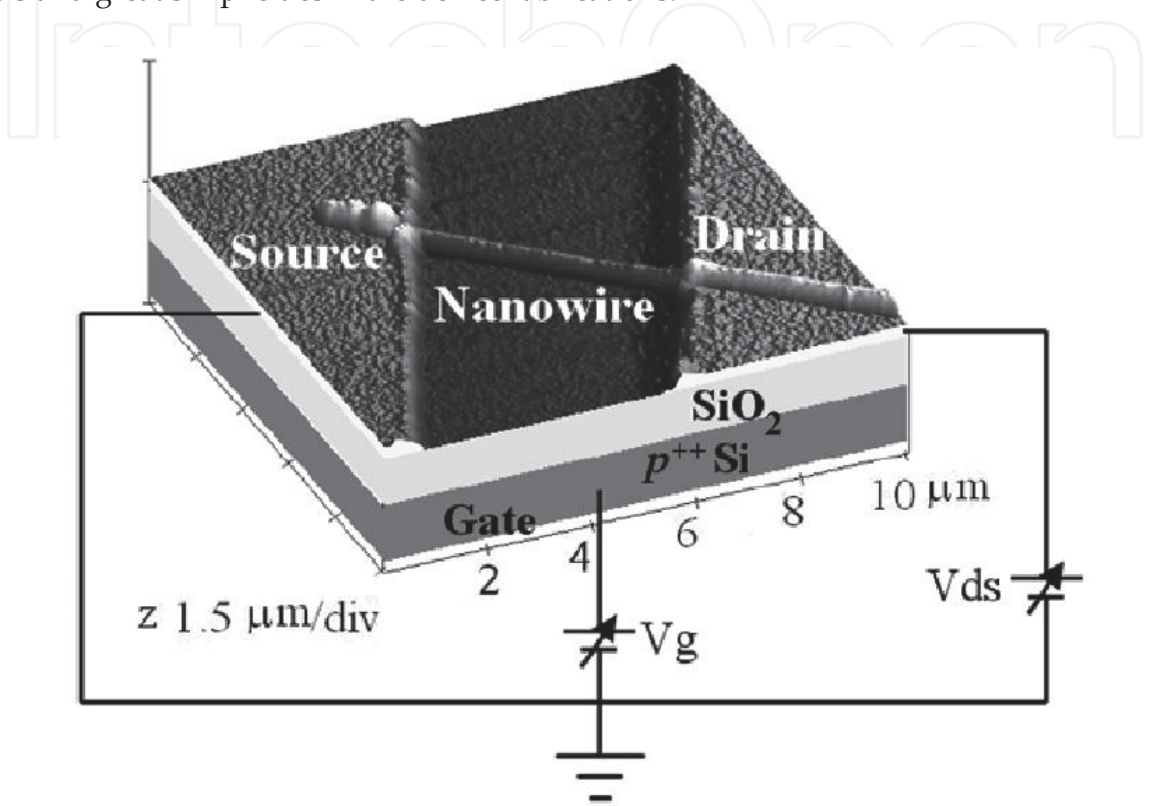
Fig. 25. Schematic of ZnO nanowire FET combined with the electrical transport measurement circuit (From Ref. [13]).
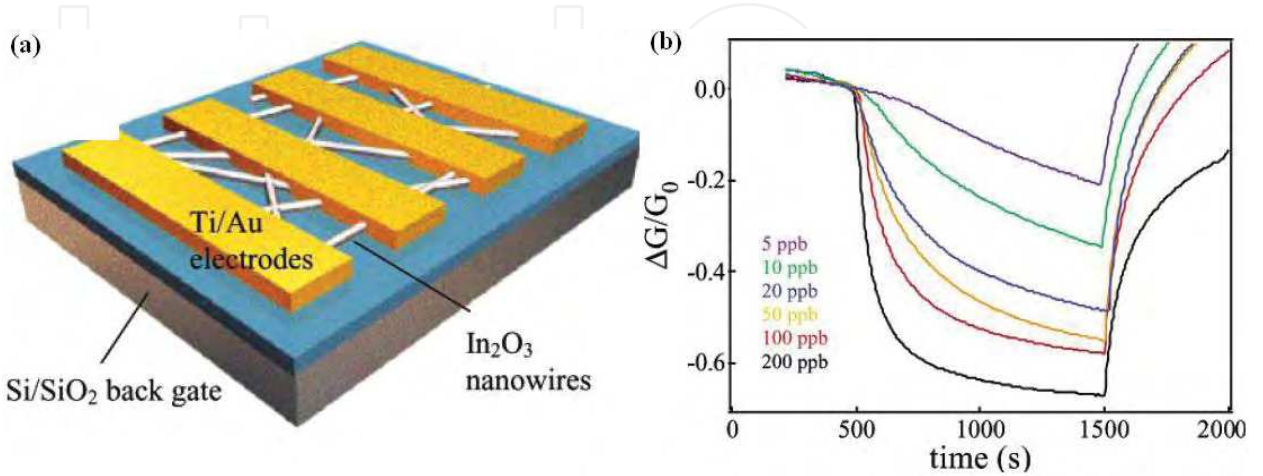
Fig. 26. (a) Schematic of a multi-nanowire FET. (b) Six sensing cycles of the multiwire device, corresponding to NO_2 concentrations of 5, 10, 20, 50, 100, and 200 ppb (From Ref. [15]).

4.2.2 Biosensors based on semiconducting oxide nanowires

Recording electrical signals from cells and tissues is a promising direction of investigations in the field of the fundamental biophysical studies and analytical biology. The combination of knowledges in bio- and electrochemistry, solid-state and surface physics, bioengineering, microelectronic technology and data processing offers the possibilities of a new generation of highly specific, sensitive, selective and reliable micro/nano-biochemical sensors and sensor arrays. Semiconductor oxide nanowires have been demonstrated as outstanding sensing-materials for the fabrications of ultra-sensitive nano-sensors due to their large surface-to-volume ratio. ZnO nanowire was tailored both physically and chemically to immobilize the enzyme glucose oxidase for construction of a glucose sensor, which was reported in the Ref. [16]. The sensor reported in this work demonstrated superior performance in sensitivities, dynamic linear range, response time, and detection limit. The high performance of the sensors was ascribed to its high specific surface area and high isoelectric point value for efficient immobilization of high concentration of acidic enzymes and the mediating effect by the redox reaction of ZnO nanowires.

FET configuration is the most typical configurations for the sensor applications. The contacts at the two ends of nanowires are usually chosen to be Ohmic contact in order to enhance the surface effect of the nanowires on the measured changes in the conductance. Wang *and co-workers* have deliberately introduced a nonsymmetric Schottky contact at one end of a ZnO nanowire device for the detection of biomolecules. A home-built microfluidic cell was placed over all biosensor devices to control the liquid environment [17]. For comparison, the Ohmic contact nanowire devices showed little changes in the electrical signals when the positively or negatively charged molecules are introduced at a concentration of 800 μg/mL. Figure 27 (a) shows a typical I-V curve of Schottky-contacted device. As shown in Figure 27 (b), a fast response and distinct current variations of Schottky-contacted nanowire biosensors can be observed when the device is exposed to a series of concentrations of negatively charged molecules. The detection limit of negatively charged biomolecules and positively charged biomolecules are as low as 2fg/mL and 20 mg/mL, respectively. They attributed the electrical response to the variation of the Schottky barrier height and barrier width as a result of biomolecule adsorption at the Schottky contact. Such nanosensors are probe-free, and it is not needed to introduce antibody–antigen interaction to enhance its sensitivity. This approach demonstrated here can serve as a guideline for designing more practical chemical and biochemical sensors.
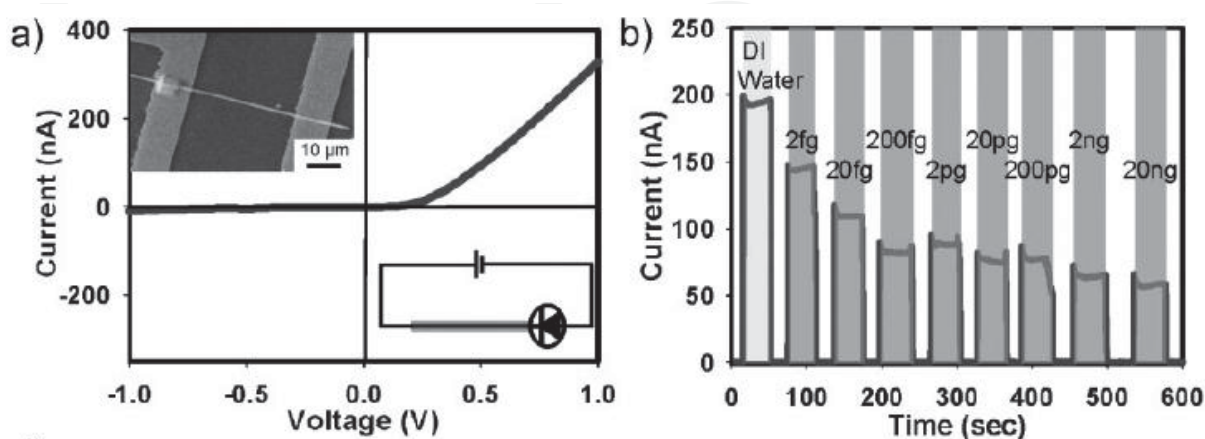

Fig. 27. (a) The I–V curve of a Schottky contact biosensor. The inset shown in upper-left is a SEM image of a Schottky contact biosensor device. (b) Current variations *vs* time curve of the sensor exposed to a series of concentrations of negatively charged molecules (From Ref. [17]).

4.3 Field Emission based on semiconducting oxide nanostructures

Field emission is based on the physical phenomenon of quantum tunneling, in which electrons are injected from the surface of materials into vacuum under the influence of an applied electric field. It is of great commercial interest in vacuum microelectronic devices such as field emission displays, x-ray sources, microwave devices, etc. One-dimensional nanosctructures such as nanotubes and nanowires are idea candidates for achieving high field emission current density at a low filed because of their high aspect ratio. In the last decade, field emission cold cathodes based on various oxide nanowires have been widely investigated.

It can be stated that within last few years, tremendous progress has already been made in field-emission applications of oxide nanowires. Here, we give some representative results on field-emission properties of ZnO nanowires reported so far. In 2002, Lee and co-workers reported the vacuum electron field emission properties of the vertically well-aligned ZnO nanowires.[74] Vertically aligned nanowires with a high density were grown on the Si substrate, as shown in Figure 28 (a). A magnified top view of nanowire array reveals that a high-purity nanowire has a sharp tip, as shown in Figure 28 (b). The synthesized ZnO nanowire indicates the average length of 13 μm and the typical diameter of 50 nm, revealing that the average aspect ratio is estimated to be larger than 250. As shown in Figure 29, the turn-on voltage of the ZnO nanowires was estimated to be about 6.0 V/μm at current density of 0.1 μA/cm². The emission current density reached 1 mA/cm² at a bias field of 11.0 V/mm. Therefore, the well-aligned ZnO nanowires grown at such low temperature can promise the application of a glass-sealed flat panel display in a near future.
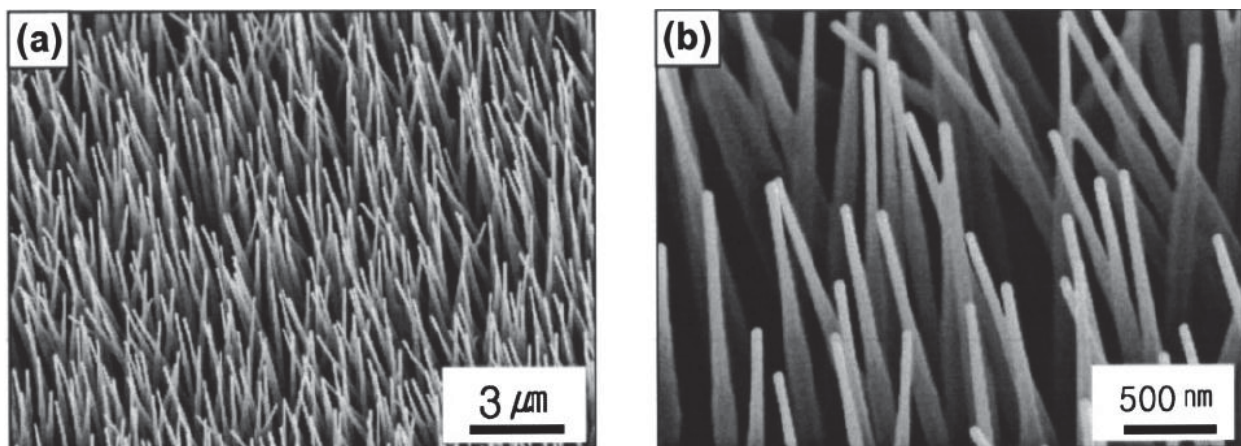

Fig. 28. SEM image of well-aligned nanowires grown on n-type silicon substrate (a) and a magnified SEM image of well-aligned nanowires (b).

2003, Yu and co-workers reported that ZnO nanoneedle arrays showed an emission current density of 2.4 mA/cm² under the field of 7 V/μm, and a very low turn-on field of 2.4 V/μm[75]. Such a high emission current density was attributed to the high aspect ratio of the ZnO nanoneedles. The high emission current density, high stability, and low turn-on field make the ZnO nanoneedle arrays one of the promising candidates for field-emission displays. In 2003, Wan and co-workers reported the synthesis and field emission properties of tetrapod-like ZnO nanostructures by thermal evaporation method via VS mechanism.[22] The field emission current versus applied electric field are shown in Figure 30 (a). The turn-on field is found to be as low as 1.6 V/μm at the current density of 1 μA/cm². The emission

current density reaches 1mA/cm² at a bias electrical field of 4.5 V/μm. The Fowler–Nordheim (F–N) plots corresponding to the data are shown in Figure 30 (b), from which the field enhancement factor β is estimated to be about 6285. ZnO nanostructures synthesized by our method are technologically useful for vacuum electron devices because they can be easily and economically synthesized and deposited on large substrates.
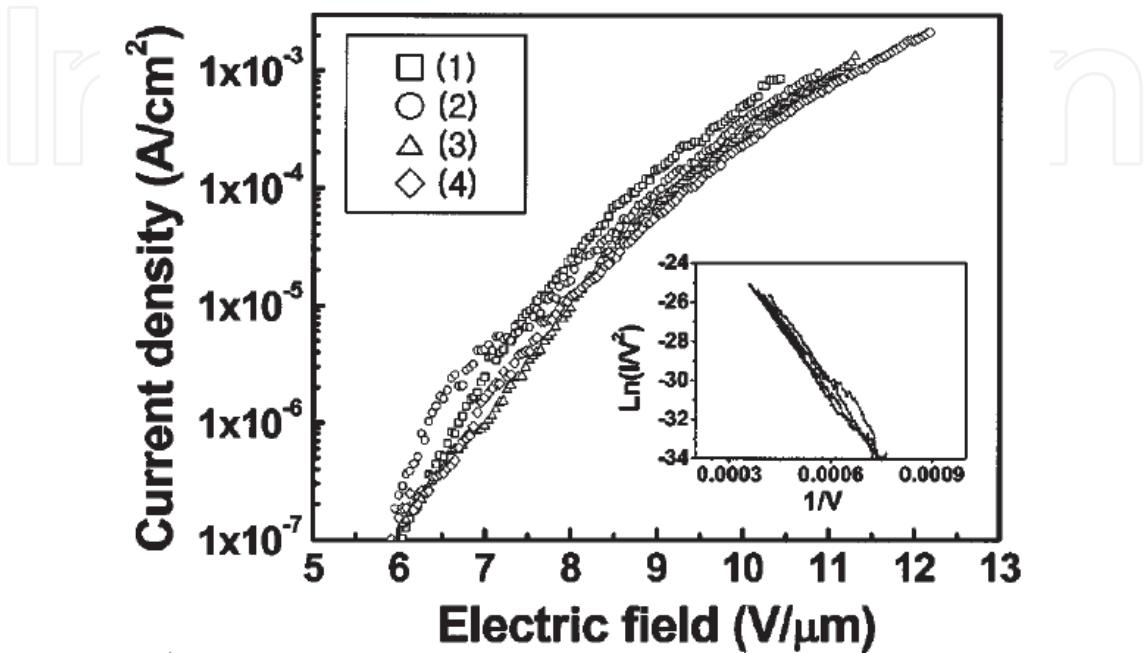

Fig. 29. Emission current density from ZnO nanowires grown on silicon substrate at 550 °C. The inset reveals that the field emission follows FN behavior.
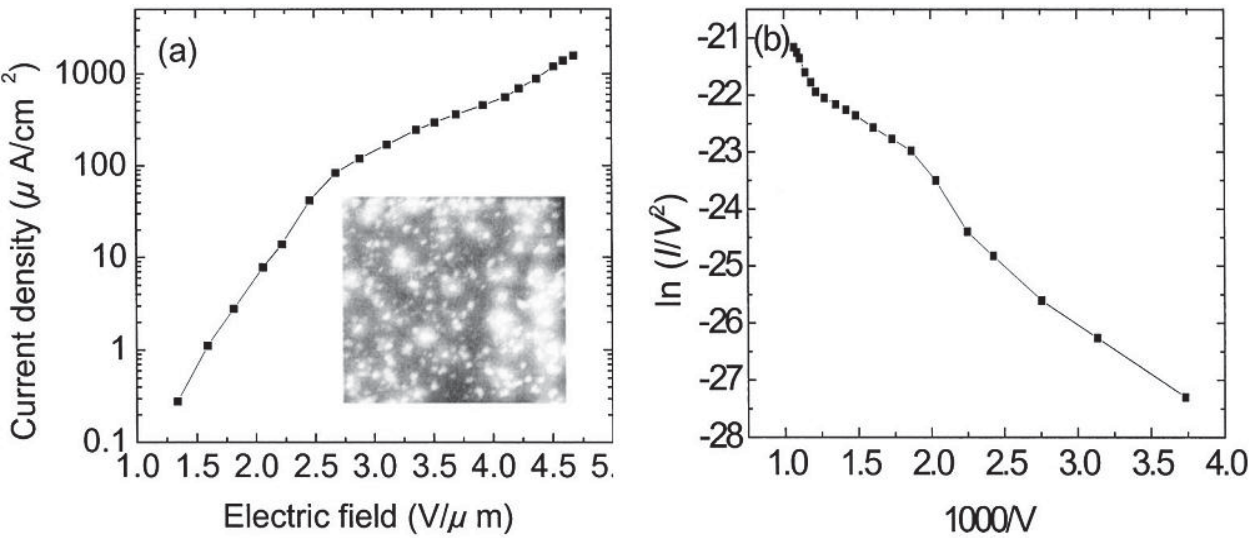
Fig. 30. The electron field emission characteristics of the tetrapod-like ZnO nanostructures. (a) The current–voltage characteristics at an anode-sample distance of 200 μm (the transparent anode image of the electron emission is shown in the inset picture) and (b) Fowler–Nordheim plot of the tetrapod-like ZnO nanostructures (From Ref. [22]).

Thermal vaporization and condensation was used to grow the ZnO nanowires on carbon cloth from a mixture source of ZnO and graphite powders in a tube furnace by Z. F. Ren and co-workers.[76] In this process, the zinc and zinc sub-oxide vapor were produced by carbothermal reduction and subsequently condensed in the lower temperature zone as the catalyst on which ZnO nanowires were grown. As shown in Figure 31, ZnO nanowire field emitters grown on carbon cloth show an extremely low operating electric field of 0.7 V/µm at an emission current density of 1 mA/cm². Such low field results from an extremely high field enhancement factor of about 4x0⁴ due to a combined effect of the high intrinsic aspect ratio of ZnO nanowires and the woven geometry of carbon cloth.
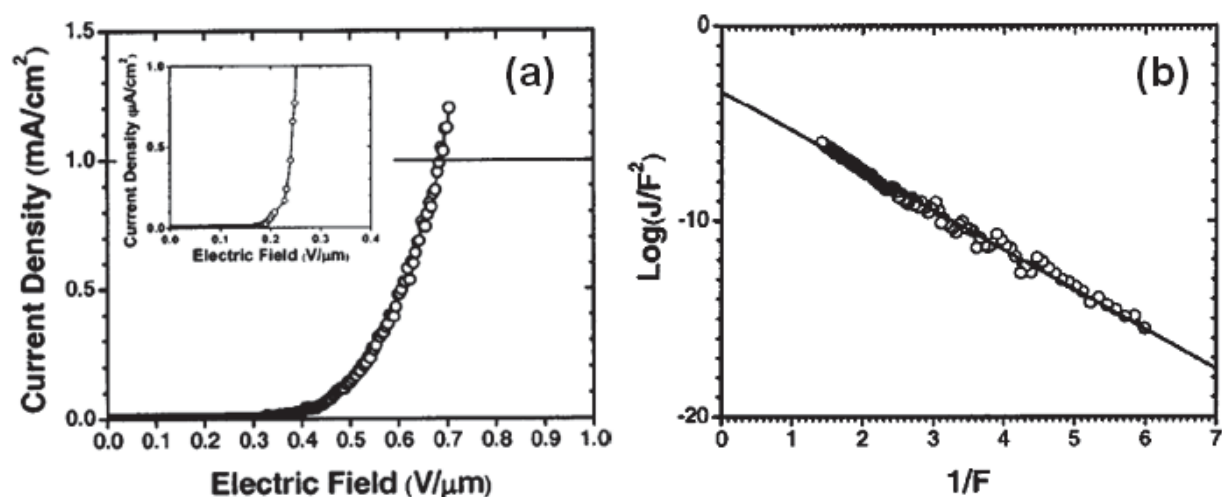
Fig. 31. The measured field emission current density of ZnO nanowires grown on carbon cloth as a function of the macroscopic electric field. The electric field required to obtain 1 mA/cm2 is 0.7 V/mm. (b) The Fowler–Nordheim plot of the field emission current density of ZnO nanowires grown on carbon cloth.

Tin-doped indium oxide (ITO) nanowires are also promising for field emitters because of their inherent properties of very low resistivities, thermally stable, and oxidation resistant. The epitaxial growth and vacuum electron field emission properties of vertically aligned ITO single-crystalline nanowire arrays on ITO/YSZ substrates have been studied by vapor transport method [23]. Figure 32 (a) shows the schematic view of our growth processes for vertically aligned ITO nanowire arrays. First, an ITO (In:Sn=95:5) buffer layer of 200 nm in thickness was deposited on (100) YSZ single-crystalline substrates (1×1 cm²) by pulsed laser deposition at 600 °C in the oxygen ambient of 2×10^{-2} Torr. A KrF excimer laser (λ =248 nm, pulse duration=20 ns, repetition frequency=5 Hz, and photon energy density=2 J/cm² pulse) was used as the laser source. ITO films grown by pulsed laser deposition method were single-crystalline with a cube-on-cube epitaxial relationship with the YSZ substrate. Subsequently, a gold film with the thickness of about 10 nm was deposited on ITO/YSZ substrates by sputtering. At last, vertically aligned ITO nanowires were grown by a vapor transport method based on the vapor-liquid-solid (VLS) growth mode, as shown by the SEM image in figure 32 (b).
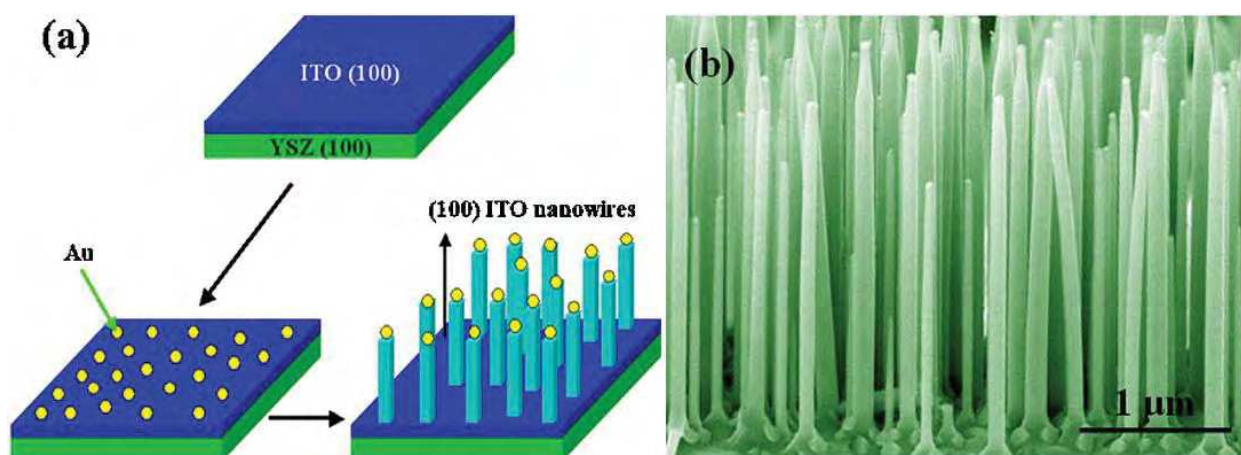
Fig. 32. (a) Schematic view of processes for vertically aligned ITO nanowire arrays grown on ITO buffer layer/(100) YSZ substrate. (b) A side-view SEM image of the vertically aligned ITO nanowires arrays grown on ITO (100) YSZ substrate (From Ref. [23]).

Field emission measurements were carried out in a vacuum chamber with the cathode-anode distance of 200 μm at room temperature. β is the field enhancement factor, E is the applied field (E=V/d), and Φ is the work function of the emission tip. Vertically aligned ITO nanowires arrays showed an enhanced field emission with a turn-on field of about 2.0 V/μm at a current density of 1 μA/cm². The β of vertically aligned ITO nanowires arrays was estimated to be bout 3850. Two curves in Fig. 35 (a) illustrate the field emission current density as a function of the applied field in semilogarithmic scale for two vertically aligned ITO nanowires arrays samples, respectively. Based on the data in Fig. 33 (a), a turn-on electrical field of about 2.0 V/μm was obtained for vertically aligned ITO nanowires arrays at a current density of 1μA/cm². Vertically aligned ITO nanowires have a stronger local electric field due to their orientation parallel to the electric-field direction. At the same time, vertically aligned ITO nanowires possess more emitter tips and the tips have better field emission performance than their bodies. Thus, vertically aligned ITO nanowire arrays show better field emission properties than randomly distributed ITO nanowires. The exponential dependence between the emission current density and the applied field indicates that the field emission from both ITO nanowire arrays follows the FN relationship, as shown in the $In(J/E^2)$-$1/E$ relationships in Fig.33 (b). From the slope of the FN curve, we can evaluate the value of β ultimately when the work function of the emission tip is known.

The field emission current dependence on vacuum pressure of the vertically aligned ITO nanowires arrays has been studied since environmental stabilities are also one of the main requirements for the practical applications. As shown in Figure 34 (a), a steady emission current density of about 2 mA/cm² was measured at the applied field of 6.0 V/μm for the vacuum level higher than 2×10^{-4}Pa. As shown in Figure 34 (b), no obvious degradations of current density are found and the current fluctuation is as low as ±5% during 2 hours continuous operation at 1×10^{-5} Pa. However, the current fluctuation becomes bigger when the vacuum level is degraded. We found that the current fluctuation was ±28% at 1×10^{-1} Pa. The emission current drops slowly in the vacuum range from 5×10^{-4} to 10^{-1}Pa. The current density at 10^{-1} Pa is about one-third of the current density at 10^{-5}Pa. A field emission

recovery was observed when ITO nanowires arrays were operated under the initial pressure of 10^{-5}Pa.
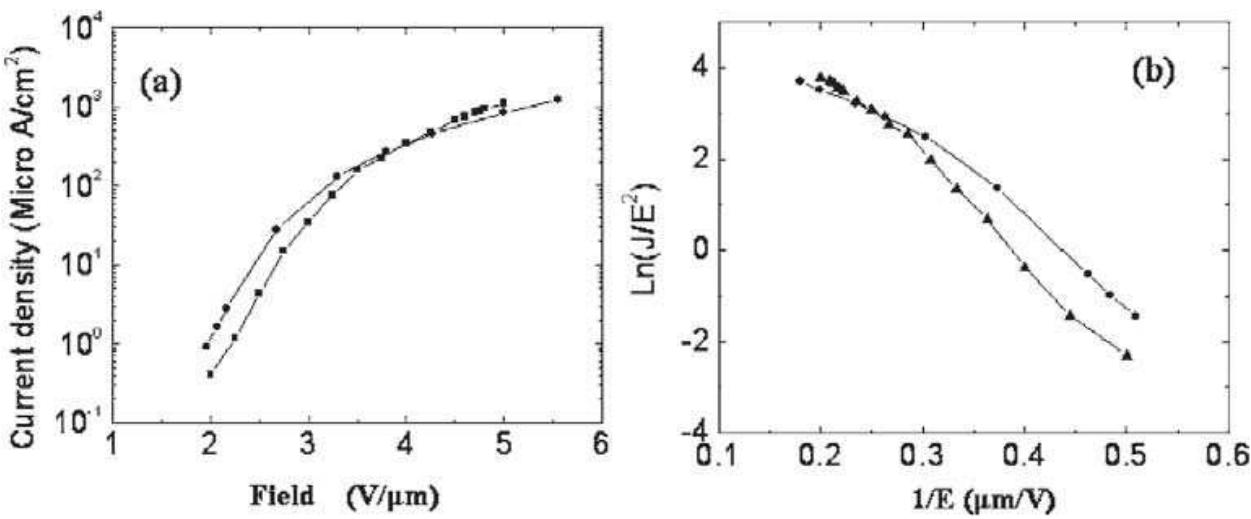

Fig. 33. (a) Field emission current density–field curves of the ITO nanowire arrays measured in the vacuum of 10^{-5}Pa. (b) The corresponding FN plots of (a) (From Ref. [23]).
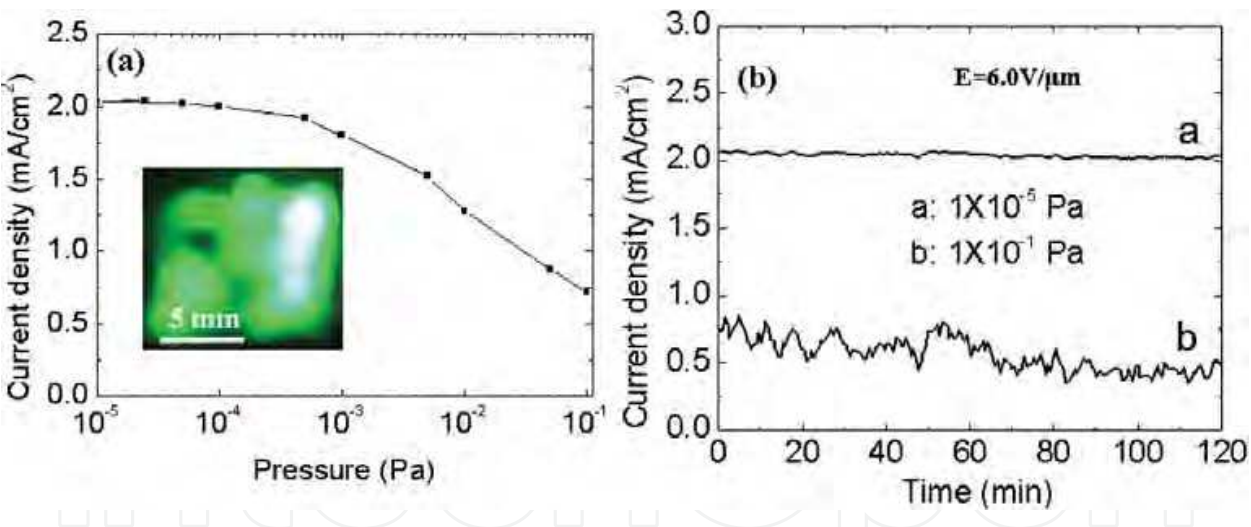

Fig. 34. (a) The dependence of emission current density of vertically aligned ITO nanowire arrays with the vacuum pressure in the range from 10^{-5} to 10^{-1}Pa. The inset shows the spatial distribution of emission of ITO nanowires at the 10^{-5}Pa. (b) Field emission current stability of ITO nanowire arrays at 10^{-5} and 10^{-1}Pa, respectively (From Ref. [23]).

These results indicate that vertically aligned ITO nanowires show relatively high environmental stabilities. Moreover, vertically aligned ITO nanowire arrays showed an enhanced field emission with a turn-on field of about 2.0 V/μm at a current density of 1 μA/cm². These results demonstrate that vertically aligned ITO nanowires arrays are very promising for vacuum electron field emission applications.

5. Summary

Semiconducting oxide nanowires, whose lateral dimensions fall anywhere in the range of 1 to 100 nm are not only interesting for fundamental research due to their unique structural and physical properties relative to their bulk counterparts, but also offer fascinating potential for future technological applications. Deeper understanding the growth, doping and applications of the oxide nanowires are central to the current research interest. This chapter has provided a comprehensive review of current research activities that concentrate on semiconducting oxide nanowires. We first gave an introduction to the synthesis and doping of semiconducting oxide nanowires. The influence of doping to the electrical and optical properties of the oxide nanowires was also described. Most attention was then devoted to the transistors, sensors and vacuum electron field emitters applications of oxide nanowires.

6. References

[1] Ju, S.; Lee, K. & Janes, D. B. "Low operating voltage single ZnO nanowire field-effect transistors enabled by self-assembled organic gate nanodielectrics," *Nano Lett.*, Vol. 5, No. 11, 2005, pp. 2281-2286.

[2] Goldberger, J.; Sirbuly, D. J.; Law, M. & Yang, P. "ZnO nanowire Transistors," J. *Phys. Chem. B*. Vol. 109, No. 1, 2005, pp.9-14.

[3] Heo, W.; Tien, L. C.; Kwon, Y.; Norton, D. P.; Pearton, S. J.; Kang, B. S. & Ren, F. "Depletion-mode ZnO nanowire field-effect transistor," *Appl. Phys. Lett.* Vol. 85, No.12, 2004, pp. 2274-2276.

[4] Ng, H. T.; Han, J.; Yamada, T.; Nguyen, P.; Chen, Y. P. & Meyyappan, M. "Single crystal nanowire vertical surround-gate field-effect transistor," *Nano Lett.* Vol. 4, No. 7, 2004, pp.1274-1252.

[5] Keem, K.; Jeong, D. Y. & Kim, S. "Fabrication and device characterization of omega-shaped-gate ZnO nanowire field-effect transistors," *Nano Lett.* Vol. 6, No. 7, 2006, pp.1454-1458.

[6] Shen, G. Z.; Chen, P. C.; Ryu, K. & Zhou, C.W. "Devices and chemical sensing applications of metal oxide nanowires" *J. Mater. Chem.*, 19, 2009, pp. 828-839.

[7] Ju, S.; Facchetti, A.; Xuan, Y. Liu, J.; Ishikawa, F.; Ye, P.; Zhou, C.; Marks, T. J. & Janes, D. B. "Fabrication of fully transparent nanowire transistors for transparent and flexible electronics," *Nat. Nanotech.* Vol. 2, 2007, pp. 378-384.

[8] Chen, P. C.; Shen, G.; Chen, H.; Ha, Y.; Wu, C.; Sukcharoenchoke, S.; Fu, Y.; Liu, J.; Facchetti, A.; Marks, T. J.; Thompson, M. E. & Zhou, C. "High-performance single-crystalline arsenic-doped indium oxide nanowires for transparent thin-film transistors and active matrix organic light-emitting diode display," *ACS Nano,* Vol. 3, No. 11, 2009, pp. 3383-3390.

[9] Zhang, F.; He, Z. B.; Yuan, G. D.; Jie, J. S.; Luo, L. B.; Zhang, X. J.; Chen, Z. H.; Lee, C. S.; Zhang, W. J.& Lee, S. T. "High-performance, fully transparent, and flexible zinc-doped indium oxide nanowire transistors," *Appl. Phys. Lett.* Vol. 94, No. 12, 2009, pp.123103.

[10] Wan, Q.; Dattoli, E. & Lu, W. "Doping-Dependent Electrical Characteristics of SnO_2 Nanowires," *small.*, Vol. 4, No. 4, 2008, pp. 451–454.

[11] Sun, J.; Liu, H. X.; Jiang, J.; Lu, A. & Wan, Q. "Low-voltage transparent SnO_2 nanowire transistors gated by microporous SiO_2 solid-electrolyte with improved polarization response." *J. Mater. Chem.*, Vol. 20, No. 37, 2010, pp. 8010-8015.

[12] Q. Wan, Q. H. Li, Y. J. Chen, and T. H. Wang, X. L. He and J. P. Li, C. L. Lin, "Fabrication and ethanol sensing characteristics of ZnO nanowire gas sensors," *Appl. Phys. Lett.*, Vol. 84, No. 18, 2004, pp. 3654-3656.

[13] Fan, Z. & Lu, J. G. "Chemical sensing with ZnO nanowire field-effect transistor," *IEEE Trans. Nanotech.* Vol. 5, No. 4, 2006, pp.393-396.

[14] Son, J. Y.; Lim, S. J.; Cho, J. H.; Seong, W. K. & Kim, H. "Synthesis of horizontally aligned ZnO nanowires localized at terrace edges and application for high sensitivity gas sensor," *Appl. Phys. Lett.* Vol. 93, No. 5, 2008, pp. 053109.

[15] Zhang, D.; Liu, Z.; Li, C.; Tang, T.; Liu, X.; Han, S.; Lei, B. & Zhou, C. "Detection of NO_2 down to ppb levels using individual and multiple In_2O_3 nanowire devices," *Nano Lett.*, Vol. 4, No. 10, 2004, pp.1919-1924.

[16] Zang, Z.; Li, C. M.; Cui, X.; Wang, J.; Sun, X.; Dong, H. & Sun, C. Q. "Tailoring Zinc oxide nanowires for high performance amperometric glucose glucose sensor," *Electroanalisis.* Vol. 19, No.9, 2007, pp.1008-1014.

[17] Zhou, J.; Gu, Y.; Fei, P.; Mai, W.; Gao, Y.; Yang, R.; Bao, G. & Wang, Z. L. "Flexible piezotronic strain sensor," *Nano Lett.* Vol. 8, No. 9, 2008, pp.3035-3040.

[18] Wan, Q.; Huang, J.; Xie, Z.; Wang, T.; Dattoli,E. N. & Lu, W. "Branched SnO_2 nanowires on metallic nanowire backbones for ethanol sensors application," *Appl. Phys. Lett.*, Vol. 92, No. 10, 2008, pp. 102101.

[19] Kuang, Q.; Lao, C.; Wang, Z. L.; Xie, Z. & Zheng, L. "High-sensitivity humidity sensor based on a single SnO_2 nanowire," *J. Am. Chem. Soc.* Vol. 129, No.19, 2007, pp. 6070-6071.

[20] Yeh, P. H.; Li, Z. & Wang, Z. L. "Schottky-gated probe-free ZnO nanowire biosensor," *Adv. Mater.* Vol. 21, No. 48, 2009, pp. 4975-4978.

[21] Das, S. N.; Moon, K. J.; Kar, J. P.; Choi, J. H.; Xiong, J.; Lee, T. I. & Myoung, J. M. "ZnO single nanowire-based UV detectors," *Appl. Phys. Lett.* Vol. 97, No. 2, 2010, pp. 022103.

[22] Wan, Q.; Yu, K.; Wang, T. H. & Lin, C. L. "Low-field electron emission from tetrapod-like ZnO nanostructures synthesized by rapid evaporation," *Appl. Phys. Lett.*, Vol. 83, No. 11, 2003, pp.2653-2655.

[23] Wan, Q.; Feng, P. & Wang, T. H. "Vertically aligned tin-doped indium oxide nanowire arrays: Epitaxial growth and electron field emission properties," Appl. Phys. Lett., Vol. 89, No. 12, 2006, pp. 123102.

[24] Lee, C. Y.; Tseng, T. Y.; Li, S. Y. & Lin, P. "Effect of phosphorus dopant on photoluminescence and field-emission characteristics of $Mg_{0.1}Zn_{0.9}O$ nanowires," *J. Appl. Phys.*, Vol. 90, No. 2, 2006, pp. 024303.

[25] Lee, C. J.; Lee, T. J.; Lyu, S. C.; Zhang, Y.; Ruh H. & Lee, H. J. "Field emission from well-aligned zinc oxide nanowires grown at low temperature," *Appl. Phys. Lett.*, Vol. 81, No. 19, 2002, pp. 3648-3650.

[26] Tseng, Y. K.; Huang, C. J.; Cheng, H. M.; Lin, I. N.; Liu, K. S. & Chen, I. C. "Characterization and Field-Emission Properties of Needle-like Zinc Oxide

Nanowires Grown Vertically on Conductive Zinc Oxide Films," *Adv. Funct. Mater.* Vol. 13, No. 10, 2003, pp.811-814.

[27] Jo, S. H.; Lao, J. Y.; Ren, Z. F.; Farrer, R. A.; Baldacchini, T. & Fourkas, J. T. "Field-emission studies on thin films of zinc oxide nanowires," *Appl. Phys. Lett.*, Vol. 83, No. 23, 2003, pp. 4821-4823.

[28] Li, S. Y.; Lin, P.; Lee, C. Y. & Tseng, T. Y. "Field emission and photofluorescent characteristics of zinc oxide nanowires synthesized by a metal catalyzed vapor-liquid-solid process," *J. Appl. Phys.*, Vol. 95, No. 7, 2004, pp. 3711-3713.

[29] Jo, S. H.; Banerjee, D. & Ren, Z. F. "Field emission of zinc oxide nanowires grown on carbon cloth," *Appl. Phys. Lett.*, Vol. 85, No. 8, 2004, pp. 1407-1409.

[30] Xia, Y. N.; Yang, P. D.; Sun, Y. G.; Wu, Y. Y.; Mayers, B.; Gates, B.; Yin, Y. D.; Kim, F. & Yan, H. Q. "One-dimensional nanostructures: Synthesis, Characterization, and Applications." vol. 15, No. 5, 2003, pp. 353-389.

[31] Wagner, R. S. & Ellis, W. C. "Vapor-liquid-solid mechanism of single crystal growth." *Appl. Phys. Lett.*, Vol. 4, No. 5, 1964, pp. 89-90.

[32] Eric, A.; Stach, P. J.; Pauzauskie,T.; Kuykendall,J.; Goldberger, R. H. & Peidong, Y. "Watching GaN Nanowires Grow" *Nano. Lett.*, Vol. 3, No. 6, 2003, pp.867- 869.

[33] Wang, Y., et al., "Catalytic Growth and Photoluminescence Properties of Semiconducting Single-Crystal ZnS Nanowires," *Chem. Phys. Lett.*, Vol. 357, No. 3-4, 2002, pp.314-318.

[34] Duan, X, & C. M. Lieber, "General Synthesis of Compound Semiconducting Nanowires," Adv. Matterials, Vol. 12, No. 4, 2000, pp. 298-302.

[35] Wan, Q.; Wei, M.; Zhi, D.; MacManus-Driscoll, J. L. & Blamire, M. G. "Epitaxial Growth of Vertically Aligned and Branched Single-Crystalline Tin-Doped Indium Oxide Nanowire Arrays," *Adv. Mater.*, Vol. 18, No. 2, 2006, pp. 234–238.

[36] Li, Q. H.; Wan, Q.; Liang, Y. X. & Wang, T. H. "Electronic transport through individual ZnO nanowires," *Appl. Phys. Lett.*, Vol. 84, No. 22, 2004, pp. 4556-4558.

[37] Chen, Y. J.; Cao, M. S.; Wang, T. H. & Wan, Q. "Microwave absorption properties of the ZnO nanowire-polyester composites," *Appl. Phys. Lett.*, Vol. 84, No. 17, 2004, pp. 3367-3369.

[38] Feng, P.; Xue, X. Y.; Liu,Y. G.; Wan, Q. & Wang, T. H. "Achieving fast oxygen response in individual β-Ga_2O_3 nanowires by ultraviolet illumination," *Appl. Phys. Lett.* Vol. 89, No. 11, 2006, pp. 112114.

[39] Feng, P.; Zhang, J. Y.; Wan, Q. & Wang, T. H." Photocurrent characteristics of individual $ZnGa_2O_4$ nanowires." *J. Appl. Phys.* Vol. 102, No.7, 2007, pp. 074309.

[40] Li, Y.; Meng, G. W.; Zhang, L. D. & Phillipp, F. "Ordered semiconducting ZnO nanowire arrays and their photoluminescence properties," *Appl. Phys. Lett.*, Vol. 76, No. 15, 2000, pp.2011-2013.

[41] Greene, L. E.; Yuhas, B. D.; Law, M.; Zitoun, D. & Yang，P. D. "Solution-Grown Zinc Oxide Nanowires," *Inorganic Chemistry*, Vol. 45, No. 19, 2006, pp.7535-7543.

[42] Li, Q. H.; Wan, Q.; Wang, Y. G. & Wang, T. H. "Abnormal temperature dependence of conductance of single Cd-doped ZnO nanowires," *Appl. Phys. Lett.* Vol. 86, No. 26, 2005, pp. 263101.

[43] Li, Q. H.; Liang, Y. X.; Wan, Q. & Wang, T. H. "Oxygen sensing characteristics of individual ZnO nanowire transistors," *Appl. Phys. Lett.*, Vol. 85, No. 26, 2004, pp. 6389-6391.

[44] Wan, Q.; Li, Q. H.; Chen, Y. J.; Wang, T. H.; He, X. L.; Gao, X. G. & Li, J. P. "Positive temperature coefficient resistance and humidity sensing properties of Cd-doped ZnO nanowires," *Appl. Phys. Lett.*, Vol. 84, No. 16, 2004, pp. 3685-3687.

[45] Wan, Q.; Lin, C. L.; Yu, X. B. & Wang, T. H. "Room-temperature hydrogen storage characteristics of ZnO nanowires," *Appl. Phys. Lett.*, Vol. 84, No. 1, 2004, pp.124-126.

[46] Feng, P.; Wan, Q.; Fu, X. Q.; Tian, Y. & Wang, T. H. "Anomalous electrorheological behavior of ZnO nanowires," *Appl. Phys. Lett.* Vol. 87, No. 3, 2005, pp. 033114.

[47] Ying, Z.; Wan, Q.; Cao, H.; Song, Z. T. & Feng, S. L. "Characterization of SnO_2 nanowires as an anode material for Li-ion batteries," *Appl. Phys. Lett.* Vol. 87, No.11, 2005, pp. 113108.

[48] Wan, Q. & Wang, T. H. "Single-crystalline Sb-doped SnO_2 nanowires: synthesis and gas sensor application," *Chem. Commun.*, No. 30, 2005, pp. 3841-3843.

[49] Liu, Z.; Zhang, D.; Han, S.; Li, C.; Tang, T.; Jin, W.; Liu, X.; Lie, B. & Zhou, C. W. "Laser Ablation Synthesis and Electron Transport Studies of Tin Oxide Nanowires," *Adv. Mater.*, Vol. 15, No. 20, 2003, pp. 1754–1757.

[50] Li, C.; Zhang, D. H.; Han, S.; Liu, X. L.; Tang, T. & Zhou, C. W. "Diameter-Controlled Growth of Single- Crystalline In_2O_3 Nanowires and Their Electronic Properties," *Adv. Mater.*, Vol. 15, No. 2, 2003, pp. 143–146.

[51] Wan, Q.; Dattoli, E. N.; Fung, W.Y.; Guo, W.; Chen, Y. B.; Pan, X. Q. & Lu, W. "High-Performance Transparent Conducting Oxide Nanowires," *Nano Lett.*, Vol. 6, No. 12, 2006, pp. 2909-2915.

[52] Huang, J.; Lu, A.; Zhao, B. & Wan, Q. "Branched growth of degenerately Sb-doped SnO_2 nanowires," *Appl. Phys. Lett.*, Vol. 91, No.7, 2007, pp. 073102.

[53] Dattoli, E. N.; Wan, Q.; Guo, W.; Chen, Y.; Pan, X. & Lu, W. "Fully Transparent Thin-Film Transistor Devices Based on SnO_2 Nanowires," *Nano Lett.*, Vol. 7, No. 8, 2007, pp. 2463-2469.

[54] Sun, J.; Tang, Q.; Lu, A.; Jiang, X. & Wan, Q. "Individual SnO_2 nanowire transistors fabricated by the gold microwire mask method," *Nanotechnology.*, Vol. 20, No. 25, 2009, pp. 255202.

[55] Liu, H. X.; Sun, J.; Tang, Q. & Wan, Q. "Ultralow-Voltage Electric Double-Layer SnO_2 Nanowire Transistors Gated by Microporous SiO_2 -Based Solid Electrolyte," *J. Phys. Chem. C,* Vol. 114, No. 28, 2010, pp. 12316–12319.

[56] Wan, Q.; Dattoli, E. N. & Lu, W. "Transparent metallic Sb-doped SnO_2 nanowires," Appl. Phys. Lett., Vol. 90, No.22, 2007, pp.22210.

[57] Pan, Z.W.; Dai, Z.R.; & Wang, Z.L."Nanobelts of semiconducting oxides", Science, Vol 291 No.5510 2001, pp.1947-1949.

[58] Wan, Q.; Song, Z. T.; Feng, S. L.; Wang, T. H.. "Single-crystalline tin-doped indium oxide whiskers: Synthesis and characterization," *Appl. Phys. Lett.*, Vol. 85, No. 20, 2004, pp. 4759-4761.

[59] Keem, K.; Kim, H.; Kim, G. T.; Lee, J. S.; Min, B.; Cho, K.; Sung, M. Y.& Kim, S. "Photocurrent in ZnO nanowires grown from Au electrodes," *Appl. Phys. Lett.*, Vol. 84, No. 22, 2004, pp. 4376-4378.

[60] Heo, Y. W.; Tien, L. C.; Norton, D. P.; Kang, B. S.; Ren, F.; LaRoche, J. R. & Pearton, S. J. "Pt /ZnO nanowire Schottky diodes," *Appl. Phys. Lett.*, Vol. 85, No. 15, 2004, pp. 3107-3109.

[61] Huang, M. H.; Wu, Y. Y.; Feick, H.; Tran, N.; Weber, E. & Yang, P. "Catalytic Growth of Zinc Oxide Nanowires by Vapor Transport," *Adv. Mater.*, Vol. 13, No. 2, 2001, pp.113-116.

[62] Kind, H.; Yan, H. Q.; Messer, B. J.; Law, M. & Yang, P. "Nanowire Ultraviolet Photodetectors and Optical Switches," *Adv. Mater.*, Vol. 14, No. 2, 2002, pp. 158-160.

[63] Kouklin, N. "Cu-Doped ZnO Nanowires for Efficient and Multispectral Photodetection Applications," *Adv. Mater.* Vol. 20, No. 11, 2008, pp. 2190–2194.

[64] Garces, N. Y.; Wang, L.; Bai, L.; Giles, N. C. & Halliburton, L. E. "Role of copper in the green luminescence from ZnO crystals," *Appl. Phys. Lett.*, Vol. 81, No. 4, 2002, pp. 622-624.

[65] Xu, C.; Sun, X. W.; Zhang, X. H.; Ke, L. & Chua, S. J. "Photoluminescent properties of copper-doped zinc oxide nanowires," *Nanotechnology*, Vol. 15, No. 7, 2004, pp. 856-861.

[66] Geng, B. Y.; Wang, G. Z.; Jiang, Z.; Xie, T.; Sun, S. H.; Meng, G. W. & Zhang, L. D. "Synthesis and optical properties of S-doped ZnO nanowires," *Appl. Phys. Lett.*, Vol. 82, No. 26, 2003, pp. 4791-4793.

[67] Qin, L.; Xu, J.; Dong, X.; Pan, Q.; Cheng, Z.; Xiang, Q. & Li, F. "The template-free synthesis of square-shaped SnO_2 nanowires: the temperature effect and acetone gas sensors," Nanotechnology, Vol. 19, No. 18, 2008, pp. 185705.

[68] Liao, L.; Zhang, Z.; Yan, B.; Bao, Q. L.; Wu, T.; Li, C. M.; Shen, Z. X.; Zhang, J. X.; Gong, H.; Li, J. C. & T. Yu, "Multifunctional CuO nanowire devices: p-type field effect transistors and CO gas sensors" Nanotechnology, Vol. 20, No. 8, 2009, pp.085203.

[69] Liu, Z.; Yamazaki, T.; Shen, Y.; Kikuta, T.; Nakatani, N. & Kawabata, T. "Room temperature gas sensing of p-type TeO_2 nanowires," Appl. Phys. Lett. Vol. 90, No. 17, 2007, pp.173119.

[70] Singh, N.; Yan, C. & Lee, P. S. "Room temperature CO gas sensing using Zn-doped In_2O_3 nanowire field effect transistors," Sens. Actuators B, Vol. 150, No.1, 2010, pp.19-24.

[71] Choi, A.; Kim, K.; Jung, H. I. & Lee, S. Y. "ZnO nanowire biosensors for detection of biomolecular interactions in enhancement mode," Sens. Actuators B, Vol. 148, No.2, 2010, pp.577-582.

[72] Das, S. N.; Kar, J. P.; Choi, J. –H.; Lee, T. I.; Moon, K. –J. & Myoung, J. –M. "Fabrication and characterization of ZnO single nanowire-based hydrogen sensor," J. Phys. Chem. C. Vol. 114, No. 3, 2010, pp.1689-1693.

[73] P. Xu, Z. Cheng, Q. Pan, J. Xu, Q. Xiang, W. Yu, and Y. chu, "High aspect In$_2$O$_3$ nanowires: synthesis, mechanism and NO$_2$ gas-sensing properties," Sens. Actuators B, Vol. 130, No.2, 2008, pp.802-808.

[74] Lee, C. J.; Lee, T. J.; Lyu, S. C.; Zhang, Y.; Ruh, H.; & Lee, H. J." Field emission from well-aligned zinc oxide nanowires grown at low temperature", *Appl. Phys. Lett.*, Vol. 81, No. 19, 2002, pp.3648-3650.

[75] Zhu, Y. W.; Zhang, H. Z.; Sun, X. C.; Feng, S. Q.; Xu, J.; Zhao, Q.; Xiang, B.; Wang, R. M. & Yu, D. P. "Efficient field emission from ZnO nanoneedle arrays," *Appl. Phys. Lett.*, Vol. 83, No. 1, 2003, pp.144-146.

[76] Jo, S. H.; Banerjee, D.; & Ten, Z. F. "Field emission of zinc oxide nanowires grown on carbon cloth", *Appl. Phys. Lett.*, Vol. 85, No. 8, 2004, pp.1407-1409.
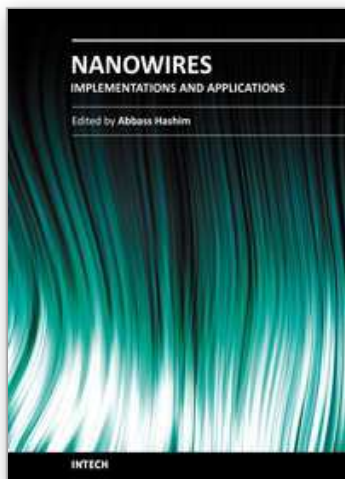
Nanowires - Implementations and Applications
Edited by Dr. Abbass Hashim

This potentially unique work offers various approaches on the implementation of nanowires. As it is widely known, nanotechnology presents the control of matter at the nanoscale and nanodimensions within few nanometers, whereas this exclusive phenomenon enables us to determine novel applications. This book presents an overview of recent and current nanowire application and implementation research worldwide. We examine methods of nanowire synthesis, types of materials used, and applications associated with nanowire research. Wide surveys of global activities in nanowire research are presented, as well.

How to reference

In order to correctly reference this scholarly work, feel free to copy and paste the following:

INTECH
open science | open minds